CHALMERS
UNIVERSITY OF TECHNOLOGY

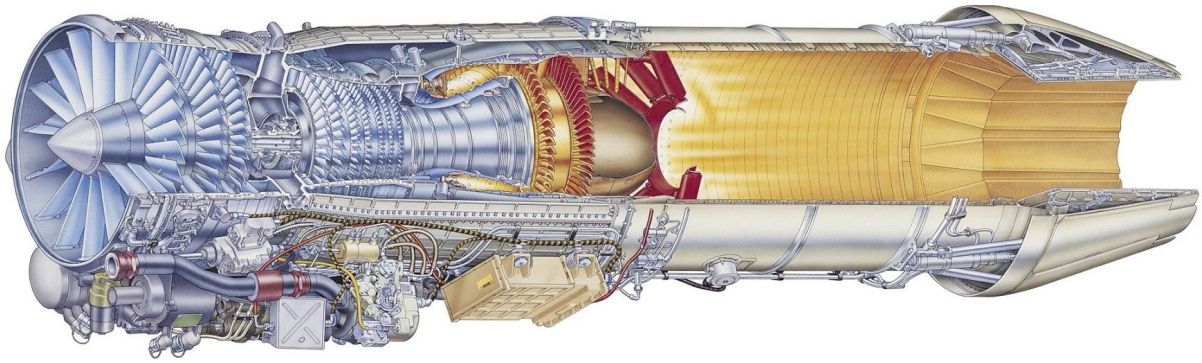

Control system design for a low bypass aircraft engine in MATLAB/Simulink

Master's thesis in Systems, Control and Mechatronics

JOHAN WALLGREN

DEPARTMENT OF ELECTRICAL ENGINEERING

CHALMERS UNIVERSITY OF TECHNOLOGY
Gothenburg, Sweden 2023
www.chalmers.se

Master's thesis 2023

Control system design for a low bypass aircraft engine in MATLAB/Simulink

JOHAN WALLGREN

CHALMERS
UNIVERSITY OF TECHNOLOGY

Department of Electrical Engineering
Chalmers University of Technology
Gothenburg, Sweden 2023

Control system design for a low bypass aircraft engine in MATLAB/Simulink
JOHAN WALLGREN

Supervisor: Dan Ring, GKN Aerospace Sweden AB
Examiner: Jonas Sjöberg, Department of Electrical Engineering at Chalmers

Master's Thesis 2023
Department of Electrical Engineering
Chalmers University of Technology
SE-412 96 Gothenburg
Telephone +46 31 772 1000

Cover: Visualization of the low bypass aircraft engine RM12 [1].

Typeset in LaTeX
Printed by Chalmers Reproservice
Gothenburg, Sweden 2023

Control system design for a low bypass aircraft engine in MATLAB/Simulink
JOHAN WALLGREN
Department of Electrical Engineering
Chalmers University of Technology

Abstract

Controlling a low bypass aircraft engine is a highly complex problem, partially because the engine characteristics of such an engine are non-linear. The control method used in this thesis is to tie multiple linear controllers together, to cover the operating range of the engine. The operating range, of the engine used in this thesis, ranges from low to high thrust levels with the engine being static at sea level altitude.

For the control design, linear engine models of the low bypass aircraft engine are derived for four different design points, throughout the operating range of the engine. The linear engine models are also scaled and reduced to improve the performance and reduce the order of the resulting controller. The inputs, outputs and control configuration for the control system are selected using methods for Control Structure Design (CSD). The linear engine models are combined with actuator models, sensor models and weighting functions to form the augmented plants for the H_∞ control design. The four multivariable linear H_∞ controllers are tied together using gain scheduling combined with bumpless transfer logic.

For evaluation, the designed control system is implemented and simulated in an existing non-linear engine model, which is a detailed dynamic simulation model based on a low bypass aircraft engine. Various simulations are performed to evaluate the performance of the control system during steady state, disturbances, transients and engine variations. The non-linear engine simulations demonstrate that the designed control system could be implemented in a real low bypass aircraft engine. However, not before all aspects to ensure safe engine operation have been considered.

Keywords: Low Bypass Aircraft Engine, MATLAB/Simulink, Multivariable Control, Engine Modelling, Model Scaling, Model Reduction, Control Structure Design (CSD), H_∞ control, Gain-scheduling, Bumpless Transfer.

Acknowledgements

I would like to thank my examiner Jonas Sjöberg from Chalmers University of Technology and Dan Ring from GKN Aerospace Sweden AB for their inputs and guidance throughout the master thesis. I would also like to additionally thank Dan Ring for taking a lot of his time to help me by providing me with suggestions and explanations along the way, his expertise and assistance have been greatly appreciated. Finally, i would like to thank Anna Lind at the "Performance and Controls" department of GKN Aerospace Sweden AB for inviting me to carry out my master thesis at her department. Anna and the employees of her department have made me feel very welcome and I have had a very enjoyable time during the course of my master thesis.

Johan Wallgren, Gothenburg, June 2023

List of Acronyms

Below is the list of acronyms that have been used throughout this thesis listed in alphabetical order:

BDPD	Block Decentralised Performance Degradation
BDRS	Block Decentralised Robust Stability
BRG	Block Relative Gain
CSD	Control Structure Design
DOF	Degree Of Freedom
ENCU	Exhaust Nozzel Control Unit
ESA	European Space Agency
FADEC	Full Authority Digital Engine Control
FCU	Fuel Control Unit
FI	Flight Idle (PLA=*28*)
GI	Ground Idle (PLA=*18*)
GKN	GKN Aerospace Sweden AB
I/O	Input/Output
IRP	Intermediate Rating Power (PLA=103)
MAX	Maximum Rating Power (PLA=130)
MIMO	Multiple Input Multiple Output
OP	Operating point
RGA	Relative Gain Array
RHP	Right Half Plane
RSCN	Robust Stability by the Conditioning Number
SLS	Sea Level Static

Nomenclature

Below is the nomenclature of the engine variables, modelling symbols and control design symbols that have been used throughout this thesis.

Engine variables

A8	Exhaust nozzle area (m^2)
CPR	Calc. compressor pressure ratio (kPa)
CVG	Compressor variable geometry (degree)
EPR	Calc. engine pressure ratio (kPa)
LPFMN	Calc. fan exit mach number (Mach)
FPR	Calc. fan pressure ratio (kPa)
FRU	Fuel ratio unit
FVG	Fan variable geometry (degree)
NH	Compressor rotor speed (rps)
NH^*	Normalised compressor rotor speed
NL	Fan rotor speed (rps)
NL^*	Normalised fan rotor speed
OPR1	Calc. compressor outlet to engine inlet pressure ratio (kPa)
PLA	Power Lever Angle (deg)
PLA^*	Estimation of the engine's current operating point (deg)
PS0	Ambient static pressure (kPa)
PS3C	Static compressor outlet pressure (kPa)
PT25	Calc. compressor inlet pressure (kPa)
PT56	Turbine downstream pressure (kPa)
TT0	Ambient temperature (K)
TT1	Fan inlet temperature (K)
TT25	Compressor inlet temperature (K)

TT31	Calc. compressor outlet temperature (K)
TT41	Calc. Turbine inlet temperature (K)
TT558	Turbine outlet temperature (K)
WFM	Main fuel flow (kg/s)
WFR	Afterburner fuel flow (kg/s)

Modelling Symbols

A	State space A matrix of engine model
A_s	State space A matrix of scaled engine model
B	State space B matrix of engine model
B_s	State space B matrix of scaled engine model
c	Compressor rotor speed conversion constant
C	State space C matrix of engine model
C_s	State space C matrix of scaled engine model
D	State space D matrix of engine model
D_s	State space D matrix of scaled engine model
G_{A8}	Exhaust nozzle area actuator model
G_{NH}	Compresor rotor speed sensor model
G_{TT558}	Turbine outlet temperature sensor model
G_{WFM}	Main fuel flow actuator model
s	Laplace variable
S_u	Input scaling matrix
S_u^{WFM}	Scaling factor of engine variable *WFM*
S_u^{A8}	Scaling factor of engine variable *A8*
S_y	Output scaling matrix
S_y^{NH}	Scaling factor of engine variable *NH*
S_y^{TT558}	Scaling factor of engine variable *TT558*
S_x	State scaling matrix
τ	Turbine outlet temperature time constant
u	Input vector
x	State vector
y	Output vector

Control design symbols

a,b,k	Weighting function constants
C	Control sensitivity function
e	Control error
γ	H_∞-norm
G	Plant transfer function
Ga	Actuator models transfer function
Gs	Sensor models transfer function
H	Bumpless transfer gain
I	Identity matrix
K	Controller transfer function
P	Augmented plant transfer function
r	Reference signal vector
rc	Measurement references
ru	Control signal references
S	Sensitivity function
t	Time constant
T	Complementary sensitivity function
u	Output signal vector/Actuator control signals
uc	Control signal reference errors
ur	Restricted control signals
u_s	Scaled output signal vector
w	External input vector
Wc	Control sensitivity weighting transfer function
$Wc_{WFM}(s)$	Control sensitivity weighting transfer function for WFM
$Wc_{A8}(s)$	Control sensitivity weighting transfer function for $A8$
Ws	Sensitivity weighting transfer function
$Ws_{NH}(s)$	Sensitivity weighting transfer function for NH
$Ws_{TT558}(s)$	Sensitivity weighting transfer function for $TT558$
Wt	Complementary sensitivity weighting transfer function
$Wt_{NH}(s)$	Complementary sensitivity weighting transfer function for NH
$Wt_{TT558}(s)$	Complementary sensitivity weighting transfer function for $TT558$
y	Output signal vector

yc	Engine measurements
y_s	Scaled output signal vector
z	Performance signals

Contents

List of Figures

List of Tables

1
Introduction

This chapter gives an introduction to the thesis by introducing the company for which this thesis is conducted in Section 1.1. Also, the low bypass aircraft engine and the engine model used in this thesis are presented in Section 1.1. Finally, the contributions are presented in Section 1.2.

1.1 Background

GKN Aerospace is the world's leading multi-technology tier 1 aerospace supplier. With 55 manufacturing locations in 15 countries, they serve over 90% of the world's aircraft and engine manufacturers. They design and manufacture innovative smart aerospace systems and components that are used in aircraft ranging from the most used civil aircraft to the world's most advanced 5th generation fighter aircraft, as well as the Ariane orbital rockets used by ESA.

The 'Performance and Controls' department at GKN Aerospace Sweden AB (GKN) is responsible for the performance and control of the low bypass aircraft engine RM12, seen in Figure 1.1, which is used in Saab JAS 39 Gripen. They have started to use MATLAB/Simulink as primary design and simulation tool package, thus requesting an evaluation of the control design tools in MATLAB/Simulink.

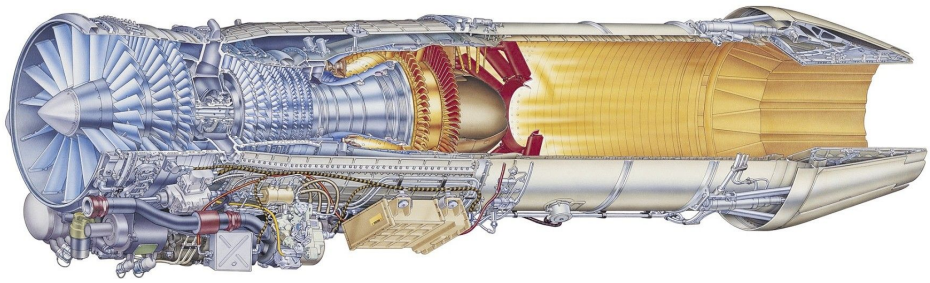

Figure 1.1: The low bypass aircraft engine RM12 [1].

The basic operation of a low bypass aircraft engine is to accelerate air to produce thrust, as described by Härefors [2]. This is done by compressing air, followed by increasing the temperature of the air through fuel burning in the core engine burner. In a low bypass aircraft engine the air is compressed in two stages, the fan and the compressor. The compressor is driven by a high pressure turbine, located directly after the core engine burner and mounted on the same shaft as the compressor.

The fan is driven by a low pressure turbine, located directly after the high pressure turbine and mounted on the same shaft as the fan. The engine is called a low bypass engine since a small amount of the air generated by the fan is passed around the compressor of the engine, known as bypass air.

Further, the low bypass aircraft engine used in this thesis is an afterburning engine. The afterburner, used to gain additional thrust by further increasing the temperature of the air through fuel burning, is located after the gas generator of the engine. The gas generator consists of the fan, compressor, core engine burner, high pressure turbine and low pressure turbine. In this thesis a detailed engine simulation model is used, developed by GKN, based on the mathematical description of the low bypass afterburning engine. The detailed engine simulation model is referred to as the existing non-linear engine model throughout the thesis.

When designing a control system for a low bypass aircraft engine, there are many aspects to take into consideration. The most important being the non-linear engine characteristics throughout the operating points of the engine. The operating points vary from low to high thrust throughout the entire flight envelope, which varies from low to high Mach numbers and from low to high altitude. However, during this thesis, only one operating point of the flight envelope is considered. That means that the engine is considered to have a constant Mach number and altitude, which is static at sea level pressure and referred to as Sea Level Static (SLS). A simplified drawing of the full flight envelope, with the marked operating point for SLS, is presented in Figure 1.2.

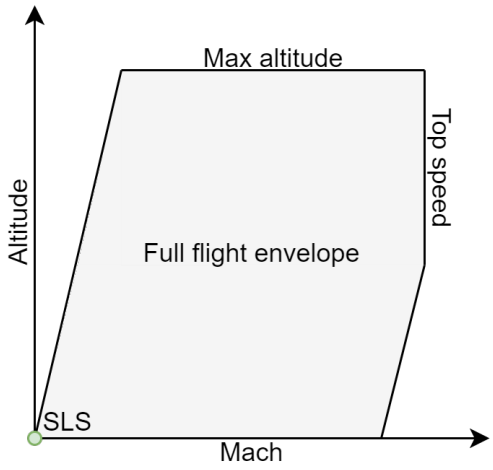

Figure 1.2: The full flight envelope, with marked operating point for SLS.

The operating points of the thrust variations, on the other hand, are determined by the Power Lever Angle (PLA). The PLA ranges from 0 to 130 degrees with the thrust level rating points Ground Idle (GI) at 18 degrees, Flight Idle (FI) at 28 degrees, Intermediate Rating Power (IRP) at 103 degrees and Maximum (MAX) at 130 degrees. The engine is turned off for PLA values below GI and the afterburner of the engine is lit for PLA values above IRP.

In the existing non-linear engine model, the engine is controlled by the Full Authority Digital Engine Control (FADEC), exactly like the real engine. To be specific the software of the FADEC, referred to as the FADEC software in this thesis, controls the engine. The FADEC software can be divided into two parts, control signal loops and actuator control loops. The control signal loops determine the demanded positions of the engine's actuators, using selected reference values of the engine outputs together with the measurement of these outputs. The actuator control loops set the actuators to the correct values, using the demanded values of the actuators together with the measured position of these actuators. Also, the FADEC software is implemented in the FADEC model of the existing non-linear engine model, making it easily interchangeable.

1.2 Contributions

- A literature survey, exploring different control strategies and different control designs applied to low bypass aircraft engines, is presented.
- A closed loop control system for a low bypass aircraft engine is designed, simulated and evaluated in MATLAB/Simulink.
- The control system is designed for the gas generator of the engine at Sea Level Static (SLS) for PLA between 18 and 103 degrees.
- The control signal loops of the control system are designed.
- The designed control system is implemented in the FADEC model of the existing non-linear engine model.

To clarify, the operating range for PLA between 18 and 103 degrees at SLS is considered to be the 'entire' operating range of the engine throughout this thesis.

2
Background of jet engine control

Theory of control systems for aircraft engines is accumulated through a literature survey, where existing control system designs are reviewed. As an introduction to the literature survey, an introduction to the control problem is given in Section 2.1. The literature survey focus on theory regarding methods for Control Structure Design (CSD) in Section 2.2, linear controllers in Section 2.3 and global controllers in Section 2.4 applied to aircraft engines. Further, a conclusion of the literature survey and the selected control concept is presented in Section 2.5.

2.1 Introduction to jet engine control

To control the low bypass aircraft engine the control variables *WFM*, *A8*, *FVG* and *CVG* are available. The fuel burning in the core engine burner is controlled by regulating the main fuel flow, called *WFM*. The engine is equipped with a variable convergent-divergent exhaust nozzle, called *A8*, which is used to control the thrust of the engine through the engine pressure ratio. The airflow in the fan and the compressor of the engine is controlled, using variable stator vanes. One set of linked variable stator vanes for the fan, called *FVG*, and one set of linked variable stator inlet vanes for the compressor, called *CVG*. These control variables are presented in Figure 2.1, which is the low bypass aircraft engine used by Härefors [3].

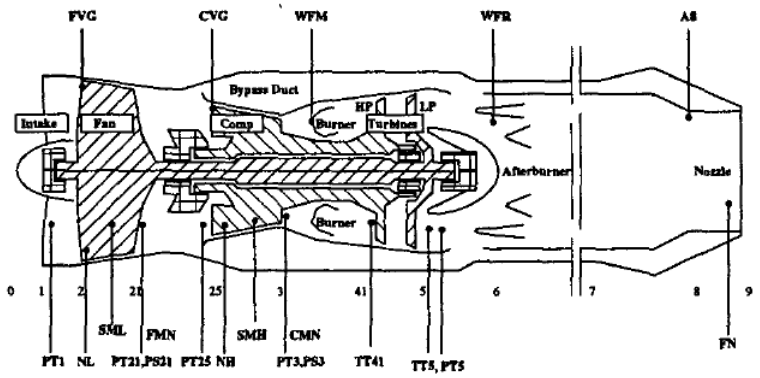

Figure 2.1: A low bypass aircraft engine with control variables and available measurements.

In some conditions, the airflow through the fan and the compressor can be disrupted and cause what is known as compressor surge. These conditions can be avoided by controlling the amount of pressure over the fan and the compressor, through *FVG*

and *CVG*. The engine could also suffer from a flameout, which is when the engine is shut off due to the extinction of the flame in the core engine burner. Fuel starvation and compressor surge are possible causes for a flameout. To ensure safe engine operation, this could be avoided by controlling the air to fuel ratios to ensure that the flame is not extinguished.

The control system design of a low bypass aircraft engine is a complex problem, partially because the engine characteristics of such an engine are non-linear, as described in Section 1.1. One approach to this problem is to design multiple linear controllers for different operating points throughout the operating range of the engine. These linear controllers are tied together to produce a control system, referred to as a global controller, that covers the entire operating range of the engine. Further, the control structure should be selected with consideration to the control design, to reduce the complexity of the control system.

2.2 Methods for control structure design

Methods for CSD were evaluated by Härefors [2], [3] in an evaluation of different engine control strategies. CSD methods were used to select inputs and outputs as well as the control law configurations for complex multivariable control systems. Further, these methods were applied to a jet engine. Also, Samar and Postlethwaite [4] performed methods for CSD on a similar jet engine.

2.2.1 I/O selection

The first method performed for Input/Output (I/O) selection by Härefors [3] was Robust Stability by the Condition Number (RSCN), which can be used for both the design-specific and the design-indipendent cases. The next I/O selection method was to select structures without Right Half Plane (RHP) zeros, since the performance of a feedback controller is likely to be limited if RHP zeros exist. The last I/O selection method was to compare the controllability and observability of different I/O-sets. This is done by calculating the Hankel singular values for the system, followed by selecting a I/O-set with high controllability and observability.

When applied to a jet engine, the inputs to the system were main fuel *WFM*, nozzle area *A8*, fan vanes *FVG*, compressor vanes *CVG* and afterburner fuel *WFR*. The outputs were chosen by performing the different I/O selection methods on the available measurements seen in Figure 2.1, i.e. RSCN, RHP zeros and Hankel singular values. The four best output-sets were the following.

- *NL*, *NH*, *FPR*, *CPR*
- *NL*, *NH*, *FPR*, *TT41*
- *NL*, *NH*, *FPR*, *EPR*
- *NL*, *NH*, *FPR*, *TT558*

NL is fan rotor speed, *NH* is compressor rotor speed, *FPR* is fan pressure ratio, *CPR* is compressor pressure ratio, *TT41* is Turbine inlet temperature, *EPR* is engine pressure ratio and *TT558* is turbine outlet temperature. However, it should be mentioned that the outputs *TT41*, *FPR*, *CPR* and *EPR* are calculated outputs.

RHP zeros and Hankel singular values were also used by Samar and Postlethwaite [4] for the I/O selection. The inputs to the system were fuel flow *WFM*, fan vanes *FVG* and nozzle area *A8*. The I/O selection methods were performed to produce the most favorable output-set, consisting of the compressor outlet to engine inlet pressure ratio *OPR1*, the fan exit Mach number *LPEMN* and the compressor rotor speed *NH*.

2.2.2 Control configuration selection

Following the I/O selection, a control configuration is selected for one of the selected I/O sets. CSD methods for control configuration selection are used to select the I/O set and the correlated control configuration.

The first method performed for control configuration selection by Härefors [3] was Relative Gain Array (RGA), which is defined as the matrix with all loop perturbations. In the ideal case, the RGA matrix is an identity matrix. Hence, configurations where the RGA matrix has diagonal elements close to one and others close to zero is preferred. The next control configuration selection method was Block Relative Gain (BRG), which is an extension of RGA that can handle block decentralised controller configurations. BRG can be used to avoid fully centralised or decentralised controllers when selecting a control configuration. Similar to RGA, the BRG matrix is preferably close to the identity matrix. The next method for control configuration selection was Block Decentralised Performance Degradation (BDPD), which is a way to measure how the controller design handles non-nominal scenarios. This is done by specifying the ideal nominal performance, followed by measuring how the controller design handles interactions that are not taken into account in the design. The final control configuration selection method was Block Decentralised Robust Stability (BDRS), which also measure the performance loss. The method predicts the stability of the block decentralised closed-loop system as well as a measurement of the performance loss due to decentralisation.

When applied to a jet engine, it turned out to be difficult to find decentralised or block-decentralised control configurations through the structure selection methods. However, BDRS produced one configuration that fulfilled the criteria when evaluating the output-set *NL*, *NH*, *FPR*, *TT558*. That produced configuration were the 3x3+1x1 configuration, with the 3x3 block $\{NL, FPR, TT558\}/\{WFM, A8, FVG\}$ and the 1x1 block $\{NH\}/\{CVG\}$.

Samar and Postlethwaite [4] also used RGA for control configuration selection. The chosen configuration was a fully decentralised controller with independent pairing of inputs and outputs. The inputs *WFM*, *FVG* and *A8* were paired with the outputs

OPR, *NH* and *FMN* respectively.

Further, Luo, Liu, Jia and Cai [5] shows a practical guideline to how control configuration selection can be performed for Multiple Input Multiple Output (MIMO) processes, where one of the methods were RGA.

2.3 Linear controllers

Sutton [6] describes an early multivariable design for a low bypass aircraft engine. The control system consists of a range controller and a NHdot, compressor rotor acceleration, controller which are combined using a control scheme. The range controller is used to regulate the control variables while the NHdot controller is used to limit large transients. That is, the NHdot controller prevents compressor surge and flameout by limiting the rate of change in the compressor. However, the main purpose of this study was to demonstrate that multivariable control is possible.

The F100 Multivariable Control Synthetis program by Szuch, Soeder, Seldner and Cwynar [7] evaluated the extension of earlier LQR work for the F100 low bypass engine. Specifically a multivariable LQR control system for the F100 engine was evaluated. The LQR controller contains a set of proportional gains, which reduce deviations in the state variables through the control variables. The proportional gains are derived by solving the Ricatti equation for a linear engine model. Further, weightings of the state variables and the control variables form a performance index, which is intended to be minimized by the LQR controller. Also, integral control can be used to control the limits of the engine. Another similar control design approach on the same engine is presented by Eisa and Tyler [8]. That control system uses linear perturbational controllers in a multivariable control system of the F100 engine. The control system was derived using the transfer function synthesis technique.

Pfeil, Athans and Spang [9] used LQR/LTR methodology to derive a multivariable control system for the T700 turboshaft engine. The LQR/LTR methodology involves shaping a loop transfer function, followed by solving the Ricatti equation for the state description of the augmented plant. Further, the intergral augmentation is included in the LQR/LTR control design.

A low order optimal controller was designed by Mahil and Bommaraja [10] for a low bypass engine. The engine was first modelled as a sixteenth-order linear dynamical model, followed by being normalised and reduced to a robust fourth-order model. The optimal controller was designed for the fourth-order model based upon a quadratic performance criterion, where the small number of quadratic weights make the controller fairly easy to tune.

Interval analysis can be used to design a robust PI controller for a jet engine, as shown by Deore and Patre [11]. The proposed controller is an NHdot controller, which allows direct control of the compressor rotor acceleration rather than compressor rotor speed. This improves transient response and reduce mechanical stress,

since tighter control of engine acceleration is possible.

Tudosie [12] extended a control system, for a two-spool jet engine, to perform coolant injection control. The original control system was an embedded control system consisting of a Fuel Control Unit (FCU) and a Exhaust Nozzel Control Unit (ENCU). A two-spool jet engine consists of one spool for low pressure and one spool for high pressure, commonly known as the fan and the compressor, respectively. A single-spool engine only consist of a compressor spool. The FCU in a single-spool engine is the same thing as a speed controller, while the engine speed of a multi-spool engine is controlled using the FCU correlated with other controllers such as the ENCU.

Another approach was used by L'Erario [13] in a control system designed for a model jet engine. That is, a single spool jet engine, used to power for example scale airplanes. Two different controllers were tested, a feedback linearization controller and a sliding mode controller. Even if the feedback linearization controller lack robustness in general, it performed better than the robust sliding mode controller. Further, an Extended Kalman Filter was used as a state observer.

Härefors [2] also evaluated some linear control design methods. Specifically, LQG, LQG/LTR, H_2 and H_∞ were evaluated. The study concluded that the H_∞ design was the most appropriate one for a low bypass aircraft engine. The H_∞ control problem is based on a 1 Degree Of Freedom (1-DOF) error feedback controller. The transfer functions used in this approach are the sensitivity function, the complementary sensitivity function and the control sensitivity function. The sensitivity function describes the process disturbance on the output, the complementary sensitivity function describes the measurement disturbance on the output and the control sensitivity function is used to track a change in reference signal or how much the control signals are put to use to undermine a disturbance. This is known as mixed-sensitivity loop shaping and was also used in the H_∞ control design by Nobakhti and Munro [14]. The control system designed by Härefors [3] was based on the H_∞ methodology to control a low bypass aircraft engine. Four weighting functions were used to shape the sensitivity, complementary sensitivity and control sensitivity functions. The selection of the weighting functions were made with consideration to the application, to obtain the desired results.

Hardt, Helton and Kreutz-Delgado [15] discussed the popularity of the H_2 and H_∞ control methodologies for jet engine applications. Their very good stabilization and robustness properties is the main reason for their continued popularity. Further, an extension to the 1-DOF H_∞ design was used by Samar and Postlethwaite [4] in a multivariable control system, designed for a Rolls Royce low bypass engine. The extension was a 2 Degrees Of Freedom (2-DOF) H_∞ linear design, used to improve the tracking performance and the robustness of the control system simultaneously. The 2-DOF H_∞ control design has also been used by Wang, Ouyang, Wang and Liu [16], where it was applied to a low bypass aircraft engine.

2.4 Global controllers

When Szuch, Soeder, Seldner and Cwynar [7] designed a control system for the non-linear engine characteristics of a low bypass engine, it was determined that a single linear controller would not provide satisfactory results in all flight conditions. Hence, a global control system was designed consisting of multiple linear controllers and switched between using gain scheduling. It was determined that six linear controllers was enough to cover the full range of power settings and flight conditions. Four linear controllers were used for high-power conditions and two linear controllers were used for low-power conditions. The gain scheduling algorithm computes a set of low- and high-power gains based on the fan inlet air density, followed by using a transition value to interpolate the low- and high-power gains. Eisa and Tyler [8] designed a similar full range non-linear transfer function controller for the F100 low bypass engine. The control system uses multiple linear controllers at different operating points and uses linear interpolation between the operating points to link them together.

Samar and Postlethwaite [4] solved the problem of designing a control system that covers the full operating range, using a gain scheduled controller. That is, multiple linear controller were designed and switched between through gain scheduling to control the engine. Gain scheduling was also used in the range controller by Sutton [6]. A similar control design was applied to a jet engine by Wang, Ouyang, Wang and Liu [16], where the flight envelope was divided into subregions based on the engine inlet parameters. In total, eight linear controllers were used to cover the full envelope of operating conditions. Further, the different linear controllers were switched, using bumpless switch logic, based on the engine altitude and Mach number. Further, even though the control system by Pfeil, Athans and Spang [9] only consists of a linear control system, the lack in performance and stability is discussed. The use of gain scheduling is mentioned as a solution for performance and stability over the full operating envelope.

The control system by Jones and Fleming [17] is a multivariable controller for an aircraft engine. The optimal control approach was used, meaning that a non-quadratic performance index directly monitors the non-linear system. Using this approach, the need for a set of linear approximations is eliminated. Further, this method enables the designer to use specific optimal controllers and penalty terms on the system inputs. However, this control system is highly dependent on the specific initial conditions and operating points, which is a significant practical disadvantage.

2.5 Conclusion

The theory accumulated about control systems for aircraft engines indicate that a good method for I/O selection is RHP-zeros. If an I/O selection of a control system has RHP-zeros, the performance of the feedback controller is likely to be limited. Also, when using CSD methods for I/O selection, a set of possible outputs for the control system is commonly selected. For control configuration selection, the RGA method is a well performing method to determine if a control system can be decentralised in some way or if a multivariable control system approach is necessary.

The literature survey indicate that the H_∞ control methodology is popular for this application, due to the very good stabilization and robustness properties. The linear H_∞ controllers used are frequently tied together using gain scheduling. There are many different approaches to the gain scheduling problem, a common being gain scheduling using bumpless transfer logic. Further, different number of linear controllers are used for the different control systems, indicating that the number of linear controllers is application specific. Thus, the best approach when selecting the number of linear controllers, to be used by the control system, is to analyse the engine characteristics of the specific engine.

The control concept chosen, to control the non-linear engine characteristics of the low bypass aircraft engine, is multiple linear controllers for different operating points. The number of linear controllers used are determined by analysing the engine characteristics of the specific engine. The linear controllers are designed using the H_∞ control methodology and tied together using gain scheduling with bumpless transfer, to produce a global controller that covers the entire operating range of the engine.

3
Engine models and linearization

This chapter presents the linear models of the low bypass aircraft engine. In Section 3.1, the linearization of the low bypass aircraft engine is described. In Sections 3.2 and 3.3, the linear engine model is scaled and reduced to improve the performance and reduce the order of the resulting controller. Following this, the selection of inputs, outputs and configuration for the control system is presented in Sections 3.4.1 and 3.4.2. The number of linear controllers selected, to cover the entire operating range of the engine, is presented in Section 3.5. Finally, the actuator and sensor models of the low bypass aircraft engine is presented in Sections 3.6 and 3.7.

3.1 Linearize engine model

The existing non-linear engine model is linearized for all available inputs and outputs using a tool developed by GKN. The tool derives a linear state space model valid around a selected operating point, using singular perturbation. That is, the linear state space model has the form seen in (3.1).

$$\begin{aligned} \Delta\dot{x} &= A\Delta x + B\Delta u \\ \Delta y &= C\Delta x + D\Delta u \end{aligned} \tag{3.1}$$

However, the Δ is removed in this thesis for simplicity and the linearized engine model is given in the state space form presented in (3.2). The input vector and output vector of the linearized engine model is described in Tables 3.1 and 3.2, respectively.

$$\begin{aligned} \dot{x} &= Ax + Bu \\ y &= Cx + Du \end{aligned} \tag{3.2}$$

Input vector	**Variable name**	**Description**
u1	*WFM*	Main fuel flow (kg/s)
u2	*A8*	Exhaust nozzle area (m^2)
u3	*FVG*	Fan variable geometry (degree)
u4	*CVG*	Compressor variable geometry (degree)
u5	*WFR*	Afterburner fuel flow (kg/s)

Table 3.1: Input vector

Output vector	Variable name	Description
y1	*TT25*	Compressor inlet temperature (K)
y2	*TT558*	Turbine outlet temperature (K)
y3	*PS3C*	Static compressor outlet pressure (kPa)
y4	*PT56*	Turbine downstream pressure (kPa)
y5	*NL*	Fan rotor speed (rps)
y6	*NH*	Compressor rotor speed (rps)
y7	*TT31*	Calc. compressor outlet temperature (K)
y8	*PT25*	Calc. compressor inlet pressure (kPa)

Table 3.2: Output vector

3.2 Model scaling

The linear engine model used is derived from the physical relations of the engine process, thus containing physical units with a wide span of magnitude. To ease the control design and improve the accuracy of the implementation, the state space model is scaled. The similar applications by Samar and Postlethwaite [4] and Härefors [2], scale the system depending on the parameters operating range. Further, Härefors [2] discusses the importance of using the same scaling throughout the entire operating range to simplify the implementation. Hence, the scaling factors are derived from the parameters operating ranges by taking the differences between the maximum and minimum values. That is, the scaling factors are the differences between IRP (PLA=103) and GI (PLA=18) for the values of all inputs, outputs and states. However, values below 1 are not desired since that would increase the scaling of the variables. To solve this, the scaling factors below 1 are set to 1 instead.

The scaling is applied, to the state space model from (3.2), as presented in (3.3).

$$\begin{aligned} A_s &= S_x^{-1} A S_x \\ B_s &= S_x^{-1} B S_u \\ C_s &= S_y^{-1} C S_x \\ D_s &= S_y^{-1} D S_u \end{aligned} \tag{3.3}$$

where S_u, S_y and S_x are diagonal matrices with the scaling factors for the inputs, outputs and states as elements, respectively. The scaled engine model is presented in (3.4).

$$\begin{aligned} \dot{x} &= A_s x + B_s u \\ y &= C_s x + D_s u \end{aligned} \tag{3.4}$$

The effect of the scaling on the singular values of the model's frequency response are shown for GI (PLA=18), PLA=60 and IRP (PLA=60) in Figure 3.1. The singular values are moved closer to each other throughout the entire operating range, but mostly in the middle of the operating range.

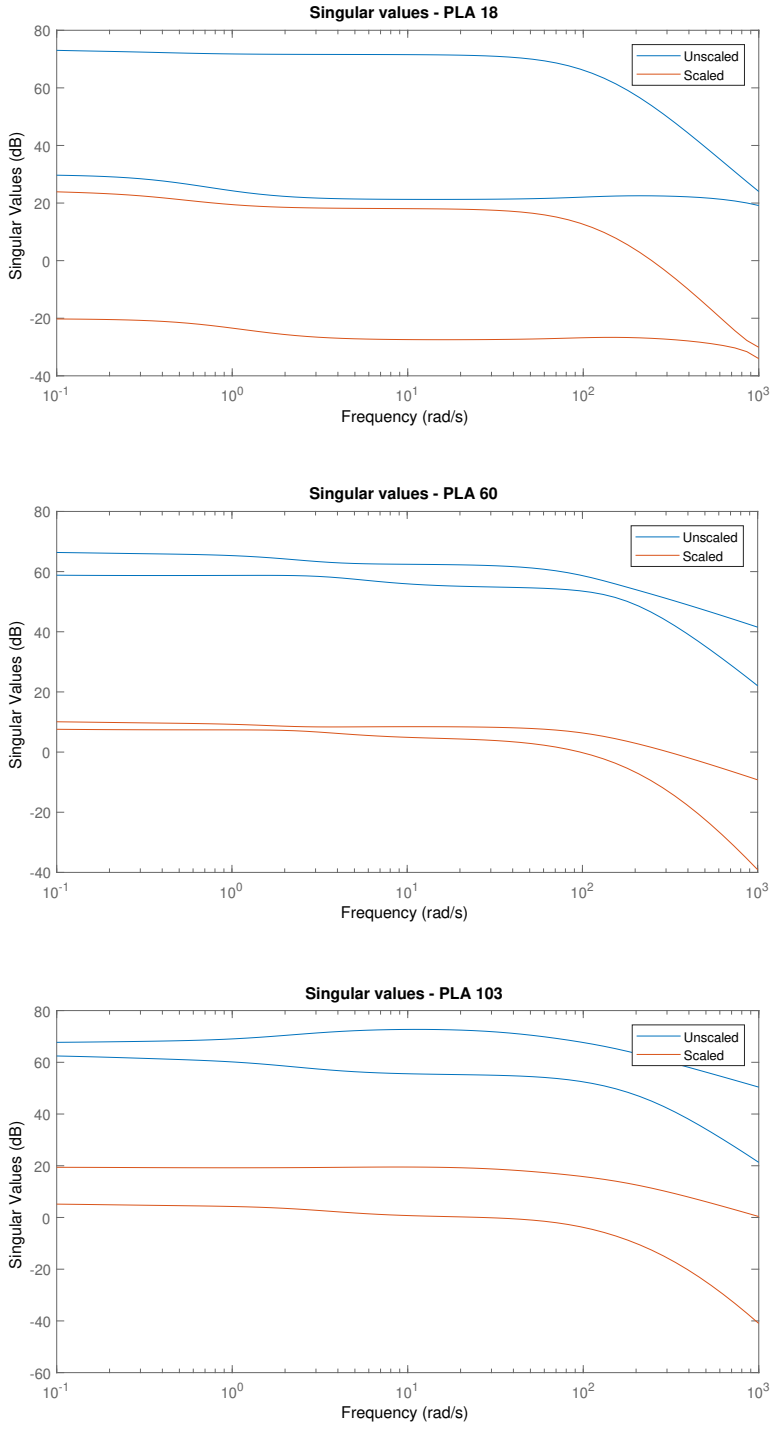

Figure 3.1: Singular values for GI (PLA=18), PLA=60 and IRP (PLA=103)

Another method to evaluate the quality of the scaling is to compute the reciprocal condition of the system, i.e. how well conditioned the system is. To estimate the reciprocal condition of the system, the MATLAB function 'rcond' [18] is used which produces a reciprocal condition number. The reciprocal condition number is computed from the A matrix of the system, giving a measure of how well the state variables are scaled. The reciprocal condition number is a value between 0 and 1, where a value near 1 indicate that the system is well conditioned. In Table 3.3, the reciprocal condition numbers are presented for the unscaled and scaled models at different operating points. Even though the condition is improved by the scaling throughout the entire operating range, the system matrices are still badly conditioned. However, the results from the model scaling is considered to be sufficient.

Operating point	**Unscaled**	**Scaled**
GI (PLA=18)	2.240231e-10	2.323589e-09
FI (PLA = 28)	3.702427e-10	2.913705e-09
PLA=40	4.353471e-10	3.809902e-09
PLA=50	4.185208e-10	4.221704e-09
PLA=60	4.937500e-10	4.966113e-09
PLA=70	7.537465e-10	7.423096e-09
PLA=80	7.234706e-10	1.058228e-08
PLA=90	7.194400e-10	1.095321e-08
IRP (PLA=103)	6.874019e-10	1.282722e-08

Table 3.3: Reciprocal condition numbers

3.3 Model reduction

The controllability and observability matrices of the engine model are not of full rank at order 33. Since a minimal form state space model is desired, the state space model is reduced. To reduce the state space model a tool developed by GKN, which partly maintains the physical interpretation of the state variables, is used to reduce the model to order 9.

The scaling of the model from the previous section has a bigger impact on the reduced model. In Table 3.4, the reciprocal condition numbers are presented for reduced unscaled and reduced scaled models at different operating points. Although, it should be noted that the system matrices are still badly conditioned even though the reciprocal condition of the system is improved.

Operating point	Reduced unscaled	Reduced scaled
GI (PLA=18)	1.290796e-08	2.370547e-04
FI (PLA = 28)	2.568321e-08	2.721806e-04
PLA=40	6.508203e-08	7.418140e-04
PLA=50	1.220673e-07	1.272345e-03
PLA=60	1.420893e-07	1.578910e-03
PLA=70	2.151342e-07	1.545418e-03
PLA=80	2.394160e-07	2.046691e-03
PLA=90	2.835426e-07	1.852764e-03
IRP (PLA=103)	3.522291e-07	2.182452e-03

Table 3.4: Reciprocal condition numbers for reduced models

However, the controllability and observability matrices of the reduced state space model are still not of full rank. To achieve minimal form of the reduced state space model, the system is further reduced. The model is reduced to order 5 using the MATLAB function 'reduce' [18], which reduces the model based on the Hankel singular values of the system. That is, the controllability and observability matrices of the further reduced engine model, of order 5, are of rank 5. Although the physical interpretations of the states are not kept using this reduction method, the reduction is considered to be small enough to not affect the results. The input vector and output vector of the reduced engine model is described in Tables 3.5 and 3.6, respectively. Note that the units of the inputs and outputs are removed because of the scaling of the engine model, described in Section 3.2.

Input vector	Variable name	Description
u1	*WFM*	Main fuel flow
u2	*A8*	Exhaust nozzle area
u3	*FVG*	Fan variable geometry
u4	*CVG*	Compressor variable geometry

Table 3.5: Reduced input vector

Output vector	Variable name	Description
y1	*TT25*	Compressor inlet temperature
y2	*TT558*	Turbine outlet temperature
y3	*PS3C*	Static compressor outlet pressure
y4	*PT56*	Turbine downstream pressure
y5	*NL*	Fan rotor speed
y6	*NH*	Compressor rotor speed
y7	*TT31*	Calc. compressor outlet temperature
y8	*PT25*	Calc. compressor inlet pressure

Table 3.6: Reduced output vector

The reduced system is analysed in both the time domain and in the frequency

domain, to confirm that the reduced model does not introduce large deviations from the full order model. Regarding the time domain, the step responses from all inputs to all outputs are analysed. Figure 3.2 presents the step responses from the two inputs *WFM* and *A8* to the output *NL*. The difference in amplitude, seen in multiple step responses, are considered to be small enough to not affect the results.

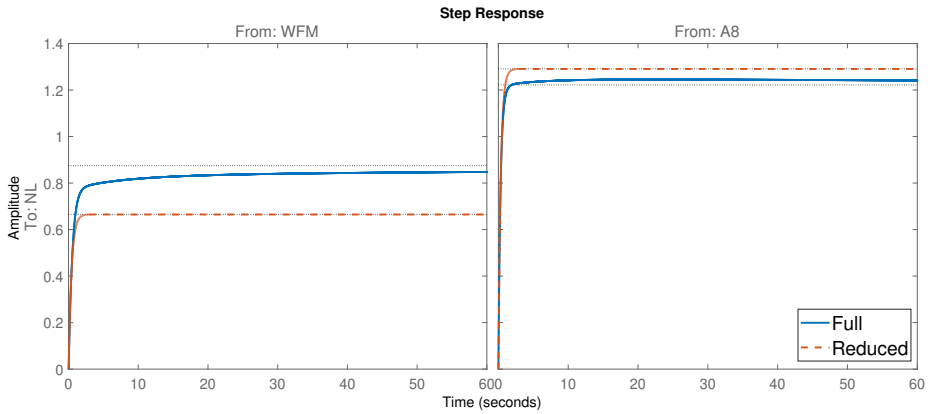

Figure 3.2: Step responses of inputs *WFM* and *A8* to output *NL*

Regarding the frequency domain, the frequency responses from all inputs to all outputs are analysed. Figure 3.3 presents the frequency response from the two inputs *WFM* and *A8* to the output *NL*. The phase drop above 100 rad/s, a trend seen in multiple frequency responses, is lost in the reduced model. However, the reduced model is still considered to be good enough for control design.

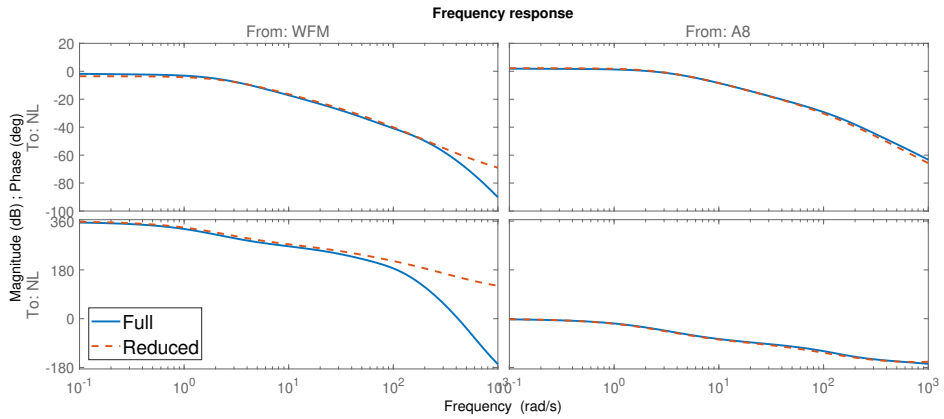

Figure 3.3: Frequency responses of inputs *WFM* and *A8* to output *NL*

3.4 Control structure design

The I/Os and control configuration of the feedback control system are selected using methods for Control Structure Design (CSD), from Chapter 2. The candidate inputs are the control variables of the engine and the candidate outputs are the measurements available on the engine. The candidate inputs and outputs for the control system of the low bypass aircraft engine are presented in Table 3.7.

Candidate inputs:		
	1	*WFM*
	2	*A8*
	3	*FVG*
	4	*CVG*
Candidate outputs:		
	1	*TT25*
	2	*TT558*
	3	*PS3C*
	4	*PT56*
	5	*NL*
	6	*NH*
	7	*TT31*
	8	*PT25*

Table 3.7: Candidate inputs and outputs for feedback control

3.4.1 I/O selection

According to Härefors [2], *WFM* and *A8* should be included in any control structure since they are the two most important control variables. *FVG* and *CVG*, however, have less importance for other engine variables and are only important to improve the operating condition of the fan and the compressor. Thus, *FVG* and *CVG* are scheduled instead of being included in the control feedback loop.

A square control system is desired for simplicity, i.e the same number of inputs and outputs. Since *WFM* and *A8* is chosen as the inputs to the feedback control system, two outputs is desired. Thus, all of the candidate outputs are paired for every combination to form 28 candidate output pairs. If there exist Right Half Plane (RHP) zeros in the system, the performance of the feedback controller could be limited. However, according to Härefors [2], a multivariable system with RHP zeros will probably only cause control problems if there exist RHP zeros at low frequencies. To avoid this, the I/O pairs that contain any RHP zeros below 100 rad/s are removed from the set of candidate outputs pairs. This reduces the number of candidate output pairs to 13.

When selecting outputs for the system, the physical aspects are also considered. The fan rotor speed and the compressor rotor speed are good indications of the operating point of the engine. Hence, at least one of the two sensors *NL* and *NH* are included in every output pair. Applying this reduces the number of candidate output pairs to 9. However, testing of different output pairs reveal that *NL* is extremely difficult to control in the lower part of the operating range. Hence, the restriction is further reduced to only include outputs pairs that contain *NH*. This reduces the candidate output pairs to the 3 presented in Table 3.8

Inputs:

1 *WFM*
2 *A8*

Possible output pairs:

1 *PT56/NH*
2 *TT558/NH*
3 *NL/NH*

Table 3.8: Selected inputs and possible output pairs

3.4.2 Control configuration selection

The control configuration selection is performed using the Relative Gain Array (RGA) on the three possible output pairs from the previous section. There are some rules of thumb when using RGA for control configuration selection, according to Härefors [2]. For decentralised control, configurations where the RGA is diagonal dominant and without any negative elements should be selected. For multivariable control, configurations were the RGA elements are small and without any negative diagonal elements should be selected. However, if the RGA matrix is not diagonal dominant or have negative diagonal elements, changing the order of the outputs can in some cases solve that issue. The RGA for the candidate output pairs are presented in (3.5), (3.6) and 3.7. Note that the order of the output pairs are changed to make the RGA matrices diagonal dominant and without negative diagonal elements.

Further, the RGA is not only important at steady-state but also for different frequencies. The rule of thumb for the frequency dependent RGA-matrix is that it should not shift sign in the frequency range of interest. Hence, RGA plots are made over a frequency range up to 50 rad/s. The RGA plots for the three output pairs are presented in Figures 3.4, 3.5 and 3.6. The presented results are for the operating point PLA=60.

Output pair 1:

$$RGA_{NH/PT56} = \begin{bmatrix} 0.9248 & 0.0752 \\ 0.0752 & 0.9248 \end{bmatrix} \tag{3.5}$$

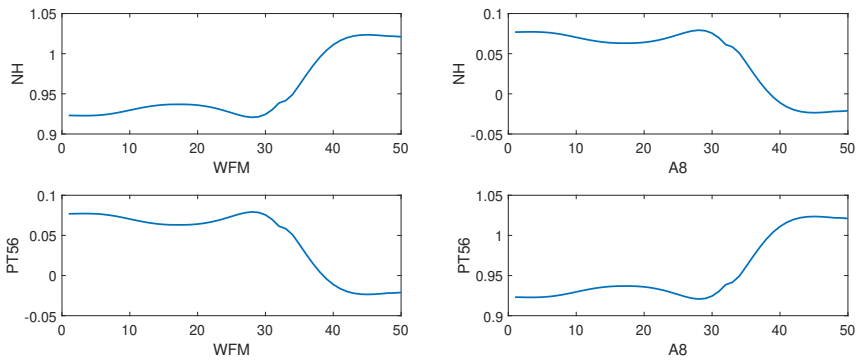

Figure 3.4: The frequency dependent RGA-matrix for *NH/PT56*

Output pair 2:

$$RGA_{NH/TT558} = \begin{bmatrix} 0.7100 & 0.2900 \\ 0.2900 & 0.7100 \end{bmatrix} \tag{3.6}$$

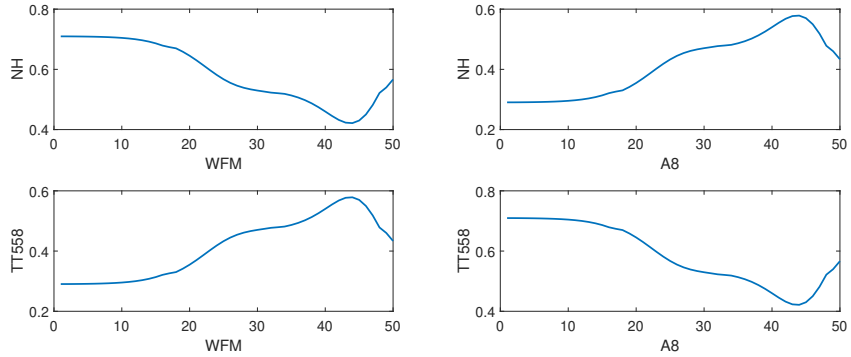

Figure 3.5: The frequency dependent RGA-matrix for *NH/TT558*

Output pair 3:

$$RGA_{NH/NL} = \begin{bmatrix} 1.2380 & -0.2380 \\ -0.2380 & 1.2380 \end{bmatrix} \tag{3.7}$$

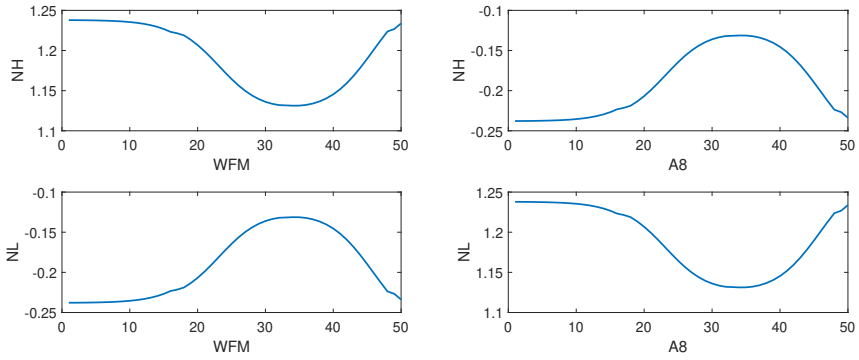

Figure 3.6: The frequency dependent RGA-matrix for *NH/NL*

The output pair *NH/PT56* has the most diagonal dominant RGA, with non-negative elements, out of the output pairs indicating very low interaction from the off-diagonal elements. However, the RGA plot reveal that the frequency dependent RGA-matrix shifts sign for high frequencies. Although, since this only occurs for the off-diagonal elements, this configuration seems to be the most suitable for decentralised control with the I/O pairing *WFM/NH* and *A8/PT56*.

Both of the configurations *NH/TT558* and *NH/NL* have small elements in the RGA-matrices, while the frequency dependent RGA-matrices does not shift sign for neither of them. The diagonal elements of the RGA-matrices are also positive. Further, the frequency dependant RGA-matrix reveals that the strong interaction between the control loops occurs through a wide range of frequencies. Thus, these configurations

seem to be more suitable for fully multivariable control. Further, since the fan rotor speed was difficult to control in the lower part of the operating range, the output pair *NH/TT558* might be the better option.

Even though a decentralised control system could be used for the feedback control system, information could be lost due to the loss of interaction between the control loops. According to Härefors [3], the best performance is achieved using multivariable control. Hence, the multivariable approach with the output pair *NH/TT558* is selected for the feedback control system. The selected control configuration is presented in Table 3.9. It should also be mentioned that this results in a multivariable compressor rotor speed controller, i.e. the speed of the compressor rotor determines the operating point of the engine.

Also, even though the presented analysis is for the operating point PLA=60, the configurations analysed in different operating points produced the same conclusion.

Inputs:		
	1	*WFM*
	2	*A8*
Outputs:		
	1	*NH*
	2	*TT558*

Table 3.9: Multivariable control configuration selected for feedback control

3.5 Design point selection

To determine how many linear controllers is sufficient, methods to find the major changes in the engine dynamics are used. To minimize the number of linear controllers, sections of the operating range with similar engine characteristics are selected. Further, the operating points that best represent the engine dynamics of the different sections are selected as design points.

To determine where the major changes in the engine characteristics occur, the engine model is linearized for the 9 different operating points GI (PLA=18), FI (PLA=28), PLA=40, PLA=50, PLA=60, PLA=70, PLA=80, PLA=90 and IRP (PLA=103). The different operating points are analysed from two different views, eigenvalue distribution and transfer functions.

The eigenvalues are analysed for both low and high frequencies. However, for the high frequency eigenvalues, the frequency simply increase with an increase in PLA. Thus, the low frequency eigenvalues indicate the major changes in engine characteristics better. Hence, the eigenvalues are presented up to 5 rad/s. The eigenvalue distribution analysis indicate that the operating range should be divided into the four sections PLA=[18,40], PLA=[40,60], PLA=[60,80] and PLA=[80,103]. This is because the major changes in the engine characteristics occur at PLA=40, PLA=60

and PLA=80. The high frequency eigenvalues for the four sections are also located reasonably close to each other. The eigenvalue distribution for the four sections can be seen in Figure 3.7.

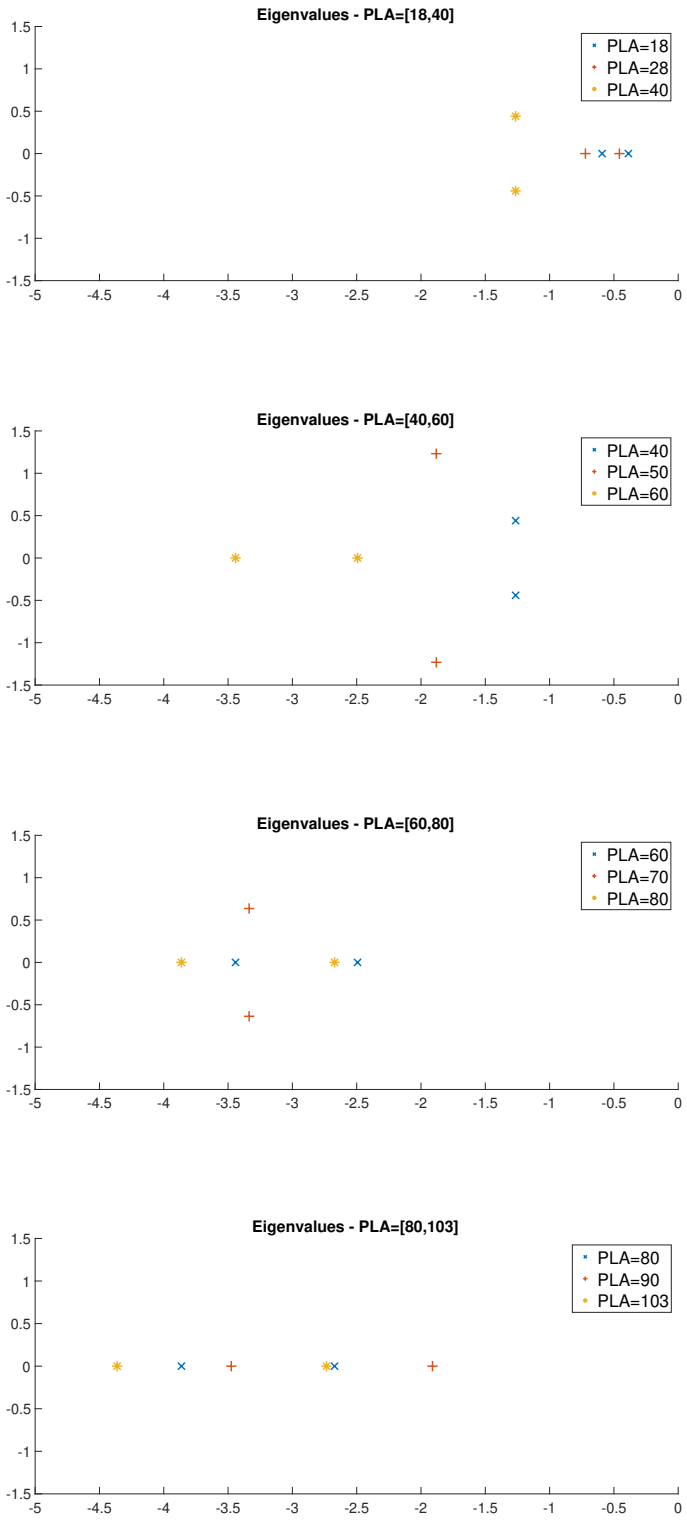

Figure 3.7: Eigenvalue distribution for the 9 operating points, divided into the four sections with similar engine characteristics

The transfer functions are also analysed for the 9 different operating points. However, since the engine is a multivariable system, the transfer function matrix would have to be analysed for every element individually. Hence, the singular values of the transfer function matrix are analysed instead, i.e the singular values of the model's frequency response. Figure 3.8 presents the singular values for the four sections from the eigenvalue distribution analysis.

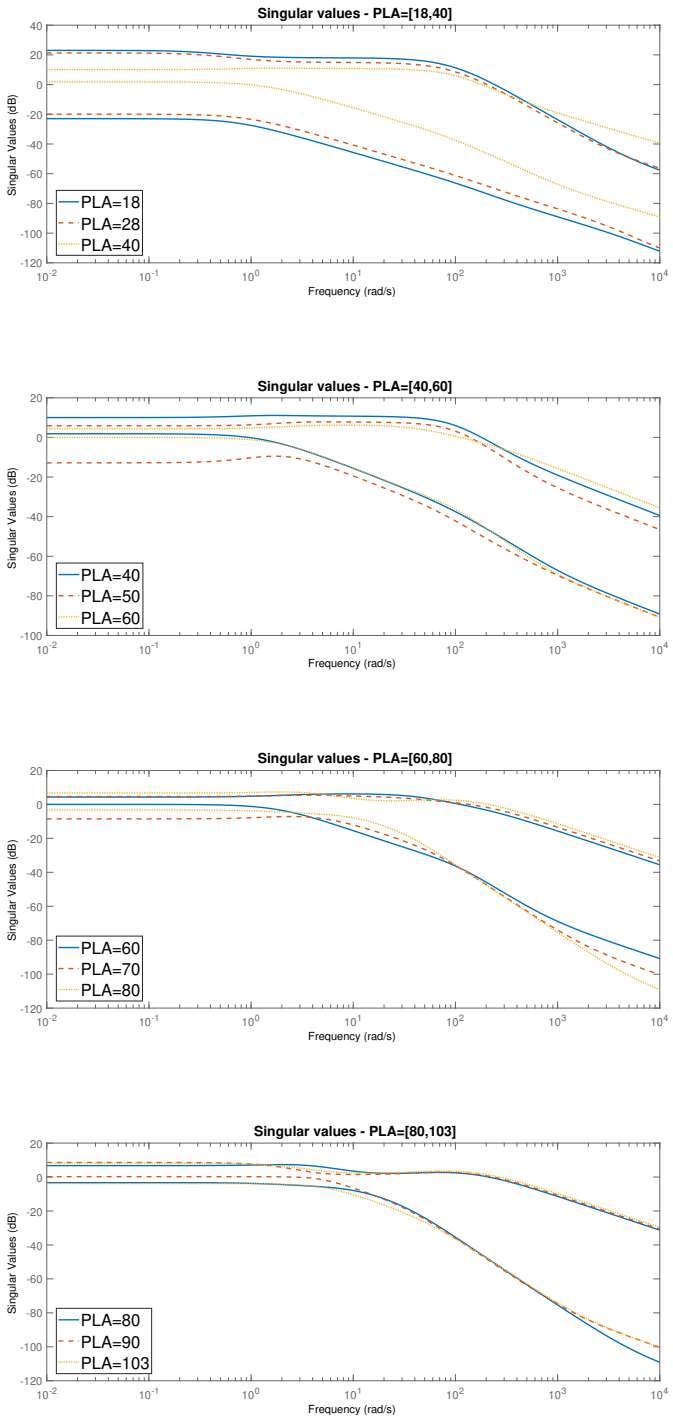

Figure 3.8: Singular values of the model's frequency responses for the 9 operating points, divided into the four sections with similar engine characteristics

The combined analysis of the eigenvalues and the singular values, for the different operating points, confirm that the major changes in the engine dynamics occur at PLA=40, PLA=60 and PLA=80. Hence, the four analysed sections are selected for the control system design.

Further, a single operating point is selected for each section as the design point. The operating points that best represent the engine dynamics of each section are located in the center of the sections. That is, the selected design points for the four sections are FI (PLA=28), PLA=50, PLA=70 and PLA=90. The selected sections of the operating range and the specific design points selected are presented in Table 3.10.

	PLA ranges	Design point (PLA)
Section 1	18-40	28
Section 2	40-60	50
Section 3	60-80	70
Section 4	80-103	90

Table 3.10: Selected design points with respective PLA ranges

3.6 Actuator models

The selected inputs to the system, *WFM* and *A8*, are actuators on the real engine. Hence, the actuators are modelled as first order filters to represent the dynamics of the real actuators. The actuator models for *WFM* and *A8* are presented in (3.8) and (3.9), respectively.

$$G_{WFM} = \frac{1}{1 + s/40} \tag{3.8}$$

$$G_{A8} = \frac{1}{1 + s/20} \tag{3.9}$$

3.7 Sensor models

The selected outputs of the system are sensors on the real engine. Hence, the sensors are modelled to represent the dynamics of the real sensors. The sensor models for *NH* and *TT558* are presented in (3.10) and (3.11), respectively. The sensor model for *NH* is a simple conversion from revolutions per second (rps) to hertz (Hz), through the compressor rotor speed converison constant c. The sensor model for *TT558* is a second order filter with one time constant τ, depending on the gas flow and temperature of the engine. The time constant for the selected design points, from Section 3.5, are presented in Table 3.11.

$$G_{NH} = c \cdot G_{NHrps} \tag{3.10}$$

$$G_{TT558} = \frac{1}{1 + s/5} \cdot \frac{1}{1 + s \cdot \tau} \tag{3.11}$$

PLA	τ
28	3.4565
50	2.1857
70	1.5795
90	1.2943

Table 3.11: *TT558* time constant for selected design points

4

Control system design

In this chapter the control system design for the low bypass aircraft engine is presented. In Section 4.1 the control requirements of the designed control system is described, followed by the general structure of the control system in Section 4.2. The design of the linear controllers, using H_∞ methodology, is presented in Section 4.3. The design of the global controller, described in Section 2.5, is presented in Section 4.4.

4.1 Control requirements

The general requirements of the controller is that the reference for *NH* should be tracked and held at steady state, to maintain the selected operating point, while the control error for *TT558* should be minimized. The control error of *TT558* is minimized to achieve smooth transients and to minimize thrust variations. The trust response of the engine is defined as the engine's response from FI to IRP, which should be 5 seconds. To accommodate this, the step response settling time of every linear controller is required to be less than 5 seconds. Further, the responses for the linear controllers is required to be as smooth as possible without any excessive overshoots. However, for the more complex controllers, PLA=28 and PLA=50, an overshoot of less than 10% of the final value is allowed.

It is required for the control system to be able to handle different types of disturbances. The disturbances could be divided into measurement disturbances and process disturbances. The measurement disturbances could be for example sensor noise, while the process disturbances could be both internal and external. Internal process disturbance could be for example fuel system disturbances, while external process disturbances could be for example intake distortion and power extraction disturbances. Also, a robust control system that handle engine variations well is required.

To ensure safe engine operation, described in Section 2.1, the control system is required to include control restrictions. Specifically, a control restriction to the fuel flow is required to limit the air to fuel ratio. Further, the mechanical hardware restrictions of the actuators on the engine are required to be included to limit the actuator control signals.

4.2 Control system structure

To give an overview of the control system, the general structure and signal flow of the system is presented in Figure 4.1.

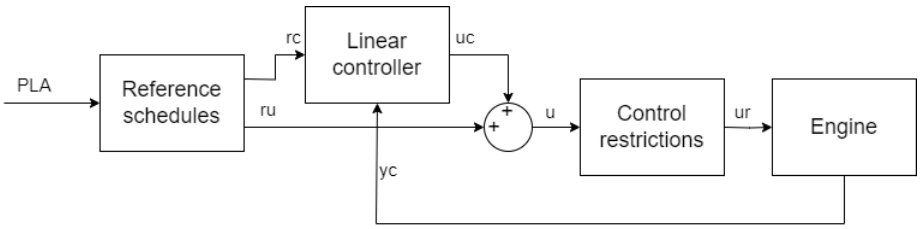

Figure 4.1: Control system structure of the designed control system

The external input *PLA* define the references of the control system in the block 'Reference schedules'. The references produced are divided into two groups, measurement references *rc* and control signal references *ru*. The control signal references act as feed forward control to the actuators of the engine, while the measurement references are used together with the engine measurements *yc* in the block 'Linear controller' to compute the control signal reference errors *uc*. The computed control signal reference errors are added to the control signal references to produce the actuator control signals *u*. Finally, the control restrictions are added to produce the restricted control signals *ur* to the engine. Note that the restricted control signals are the demanded values of the engine's actuators used in the actuator loops, described in section 1.1, which are included in the block 'Engine'.

The block 'Reference schedules' is presented in Section 4.4.1. The block 'Linear controller' includes all of the linear controllers as well as the gain scheduling with bumpless tranfer. Hence, the block 'Linear controller' is described in Sections 4.3, 4.4.2 and 4.4.3. Finally, the block 'Control restrictions' is presented in Section 4.4.4.

4.3 Linear control design

The linear controllers for the selected design points, described in Section 3.5, are designed using the same methodology. In this section, the linear control design for the operating point PLA=90 is thoroughly described.

4.3.1 Control objectives

During the system analysis and control design, the transfer functions of interest are the sensitivity function S the control sensitivity function C and the complementary sensitivity function T. This method is known as mixed-sensitivity design, as presented in Section 2.3. The definition of these transfer functions are presented in (4.1), (4.2) and (4.3), where I is the identity matrix, G is the plant and K is the controller.

$$S = (I + GK)^{-1} \tag{4.1}$$
$$C = KS = K(I + GK)^{-1} \tag{4.2}$$
$$T = (I - S) = (I + GK)^{-1}GK \tag{4.3}$$

The sensitivity function is the transfer function from the reference r to the control error e. It is also often used to describe the influence of process disturbance on the output y. Also, to avoid amplification of disturbances, it is desirable to not have any amplification in the control loops used for reference tracking below the bandwidth.

The control sensitivity function is the transfer function from the reference r to the control signals u. It is used to describe how much the control signals are used to track a change in reference values, or to reduce a disturbance. The mechanical hardware restrictions of the engine's actuators, described in Section 4.1, are used to define the control sensitivity function.

The complementary sensitivity function is the transfer function from the reference r to the output y. It is also often used to describe the influence of measurement disturbance on the output y. Thus, the complementary sensitivity function should be small for high frequencies to attenuate for measurement disturbances.

4.3.2 Design method

The general representation of the H_∞ design method is presented in Figure 4.2, where *P(s)* is the augmented plant and *K(s)* is the controller.

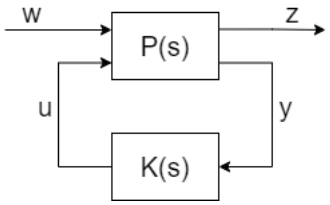

Figure 4.2: General H_∞ control design representation

The external inputs w are the reference values r in this thesis. The performance signals z contain the performance criteria for the system. That is, the performance signals contain the weighted outputs that are optimised by the H_∞ controller. Further, the measured variables y and the control signals u are the inputs and outputs to the H_∞ controller. The H_∞ control design, translated to the low-bypass aircraft engine, is presented in Figure 4.3. Note that the actuator and sensor models, described in sections 3.6 and 3.7, are added to the augmented plant.

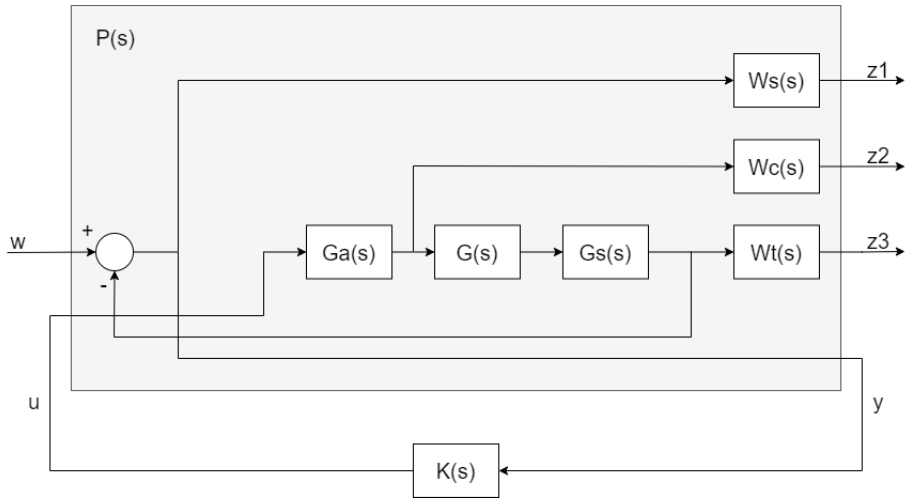

Figure 4.3: H_∞ control design for the low-bypass aircraft engine

G(s) is the linearized engine model from Chapter 3 for the current operating point, *PLA*=90, given in state space form. *Ga(s)* is the actuator models and *Gs(s)* is the sensor models from Chapter 3, represented as diagonal transfer function matrices. Further, *P(s)* is the augmented plant for the low-bypass aircraft engine.

The weighting function *Ws(s)* is used to shape the sensitivity function, while the weighting function *Wt(s)* is used to shape the complementary sensitivity function. *Wc(s)* is the weighting function used to shape the control sensitivity function. The weighting functions are written as diagonal transfer function matrices.

The augmented plant is implemented in MATLAB and the function *'hinfsyn'*, from the robust control toolbox [19], is used to compute the H_∞ controller. The H_∞ controller minimizes the criteria described in (4.4). Härefors [2] performs a detailed derivation of the minimization criteria from the sensitivity weighting functions. Note that S, C and T have the same shape as the inverse of the respective weighting functions.

$$\|F_l(P,K)\|_\infty = \left\| \begin{bmatrix} WsS \\ WcC \\ WtT \end{bmatrix} \right\|_\infty \leq \gamma \tag{4.4}$$

4.3.3 Selecting the weighting functions

Low order weighting functions are desired, since the resulting controller have the same order as the augmented plant. To keep the order of the weighting functions as low as possible only first order weights are used, on the form given by (4.5). Further, to meet the response requirements from Section 4.1, a bandwidth of at least 1 rad/s is selected for the *NH* control loop.

$$W = k\frac{s+b}{s+a} \tag{4.5}$$

Since good reference tracking of *NH* is desired, integral action is implemented in this control loop. Integral action, or low sensitivity, is implemented in the control loop by making $Ws_{NH}(s)$ large at low frequencies. For the *TT558* control loop a high sensitivity is selected by making $Ws_{TT558}(s)$ a small constant, otherwise known as a static gain, since no reference tracking is required. The weighting function for the sensitivity function are presented in (4.6) and the inverse of the individual weighing functions are presented in Figure 4.4.

$$Ws(s) = \begin{bmatrix} Ws_{NH}(s) & 0 \\ 0 & Ws_{TT558}(s) \end{bmatrix} = \begin{bmatrix} \frac{1}{50}\frac{s+5}{s+0.001} & 0 \\ 0 & 0.001 \end{bmatrix} \tag{4.6}$$

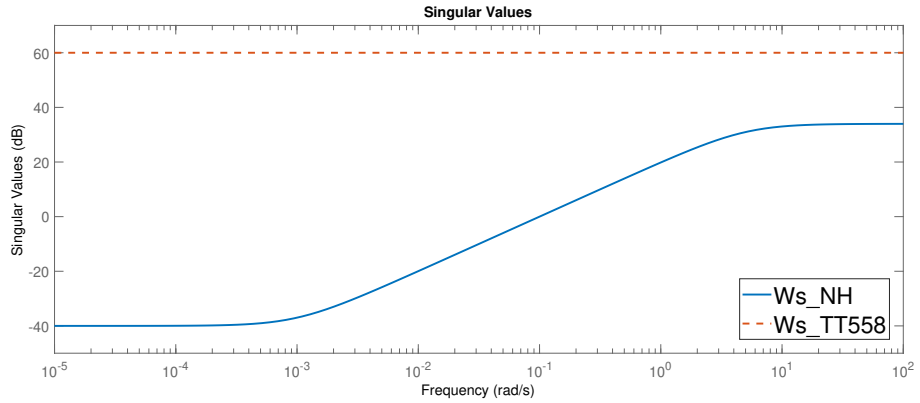

Figure 4.4: Individual weightings of the inverse weighting function $Ws(s)^{-1}$

To model the hardware limitations of the actuators on the engine, the weighting function *Wc(s)* is selected through static gains. The weighting function for the control sensitivity function are presented in (4.7) and the inverse of the individual weighing functions are presented in Figure 4.5.

$$Wc(s) = \begin{bmatrix} Wc_{WFM}(s) & 0 \\ 0 & Wc_{A8}(s) \end{bmatrix} = \begin{bmatrix} \frac{1}{1.8} & 0 \\ 0 & \frac{1}{8} \end{bmatrix} \tag{4.7}$$

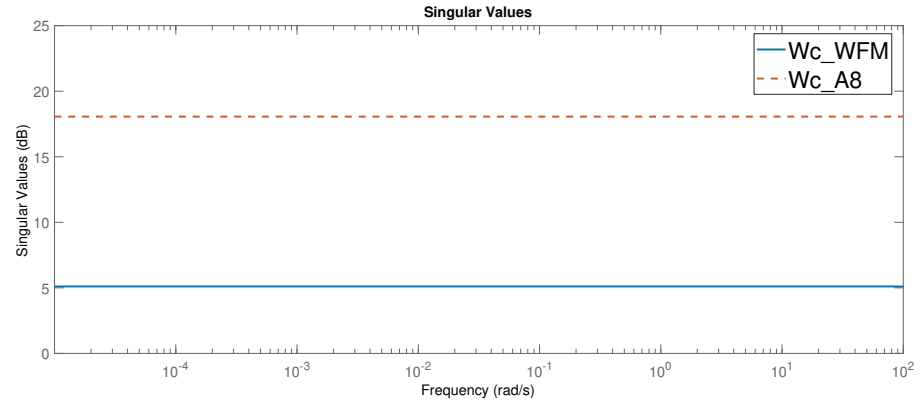

Figure 4.5: Individual weightings of the inverse weighting function $Wc(s)^{-1}$

To attenuate measurement disturbances of the *NH* control loop, low complementary sensitivity is selected for high frequencies by setting $Wt_{NH}(s)$ to be large at high frequencies. For the *TT558* control loop a low complementary sensitivity is selected, to attenuate measurement disturbances, by making $Wt_{TT558}(s)$ a large static gain. The weighting function for the complementary sensitivity function are presented in (4.8) and the inverse of the individual weighing functions are presented in Figure 4.6.

$$Wt(s) = \begin{bmatrix} Wt_{NH}(s) & 0 \\ 0 & Wt_{TT558}(s) \end{bmatrix} = \begin{bmatrix} 40\frac{s+0.001}{s+2.5} & 0 \\ 0 & 1000 \end{bmatrix} \tag{4.8}$$

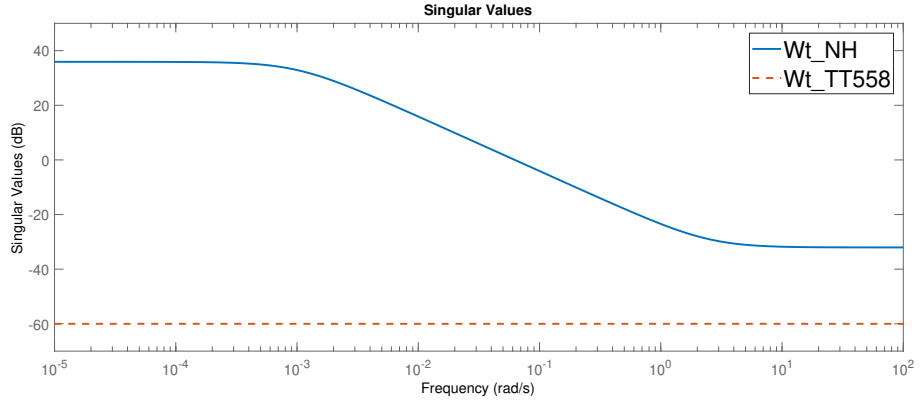

Figure 4.6: Individual weightings of the inverse weighting function $Wt(s)^{-1}$

The resulting sensitivity function and complementary sensitivity function from the selected weighting functions is seen in Figure 4.7. The figure presents the singular values of the sensitivity and complementary sensitivity function with the H_∞-norm, presented in (4.4), which is $\gamma = 1.7435$.

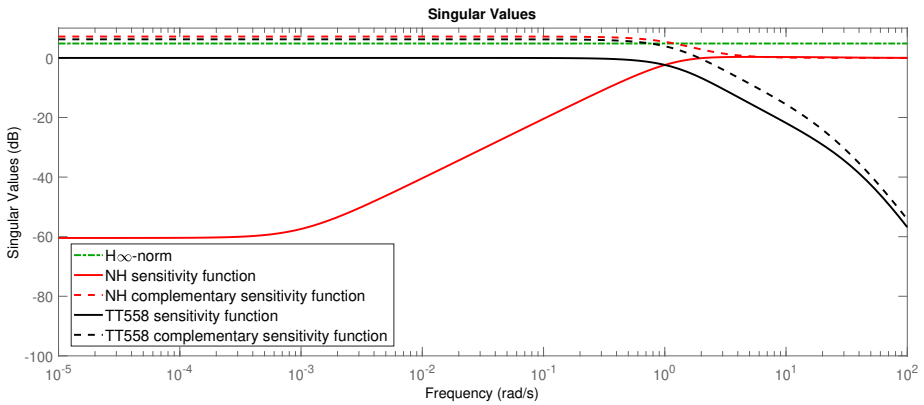

Figure 4.7: Singular values of the sensitivity and complementary sensitivity function

4.3.4 Evaluation

Figure 4.8 presents the frequency response of the sensitivity function and complementary sensitivity function with the transfer loop and plant transfer functions. The loop transfer has high gain below the bandwidth for both outputs of the *NH* control loop and low gain above the bandwidth for all outputs. This indicate that good reference tracking is achieved for the *NH* control loop and that good disturbance attenuation is achieved for both control loops. The achieved bandwidth for NH is 1.1558 rad/s. Further, the controller does not contain any *rhp* zeros indicating that the controller is stable.

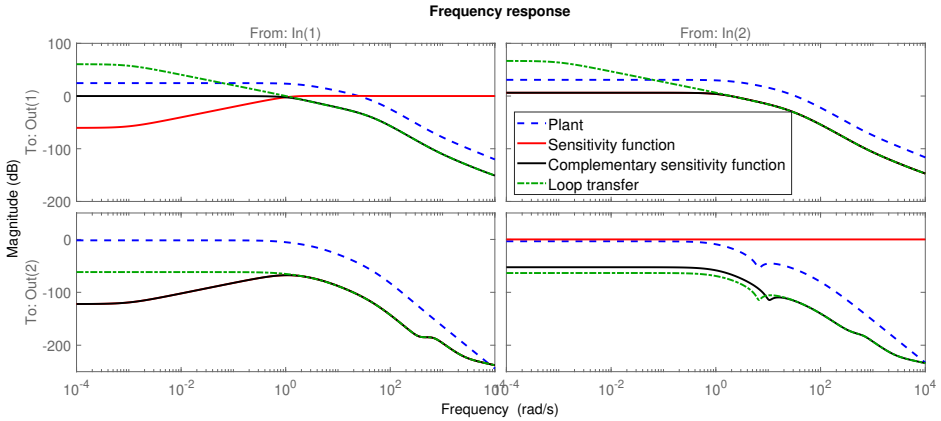

Figure 4.8: Frequency responses of sensitivity function and complementary sensitivity function with the transfer loop and plant transfer functions

To further evaluate the linear controller a step response on *NH* is performed, seen in Figure 4.9. The horizontal dashed line indicate the maximum overshoot allowed, while the two vertical dashed lines indicate the maximum settling time allowed for *NH*. As seen, the linear controller meets these requirements while the control error of *TT558* is minimized reaching a maximum value of less than 1/20 of *NH*.

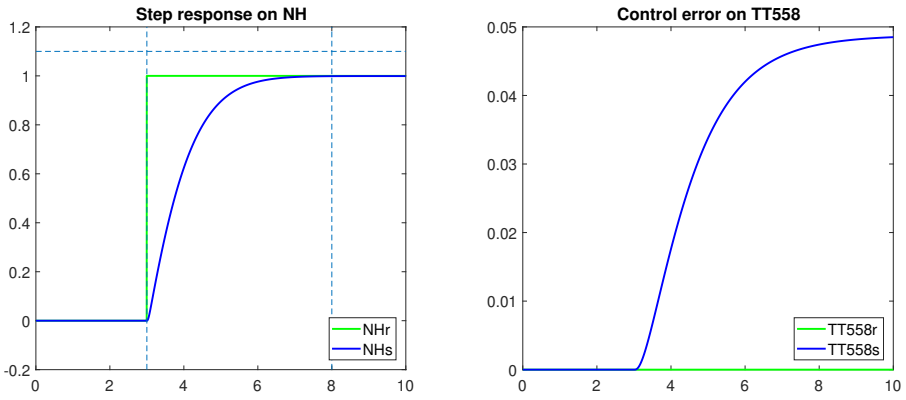

Figure 4.9: Step response on *NH* for *PLA*=90 controller

To evaluate the robustness of the linear controller the time constants of the actuator models, G_{WFM} and G_{A8}, and the *TT558* sensor model, G_{TT558}, are varied. How

much the time constants are varied is presented in Table 4.1. All configurations are tested, but the configuration where the time constants are 10% smaller for G_{WFM}, 50% smaller for G_{A8} and 20% smaller for G_{TT558} is presented. The frequency response of the sensitivity function and complementary sensitivity function with the transfer loop and plant transfer functions is presented in Figure 4.10, while the step response is presented in Figure 4.11. Note that the performance of the controller is very similar to the nominal performance, indicating that a robust controller is achieved.

Transfer function	**Time constant variation**
G_{WFM}	$\pm 10\%$
G_{A8}	$-50\% + 100\%$
G_{TT558}	$\pm 20\%$

Table 4.1: Variations of actuator and sensor model time constants

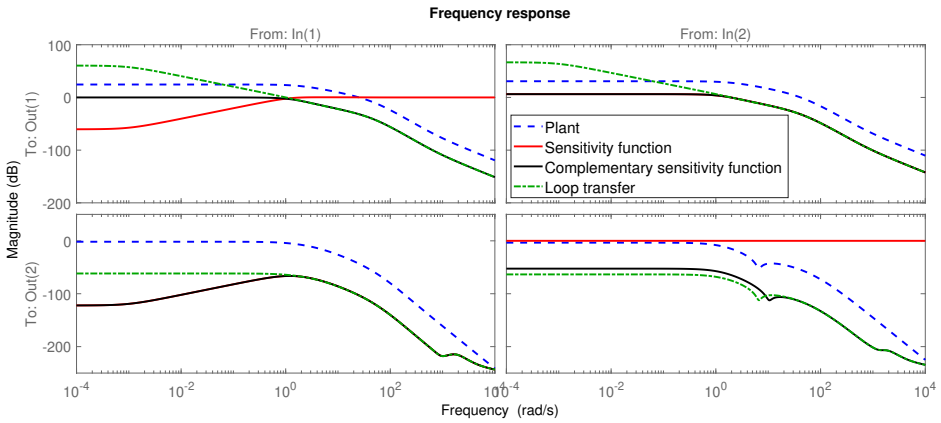

Figure 4.10: Frequency responses of sensitivity function and complementary sensitivity function with the transfer loop and plant transfer functions, where the time constants are 10% smaller for G_{WFM}, 50% smaller for G_{A8} and 20% smaller for G_{TT558}

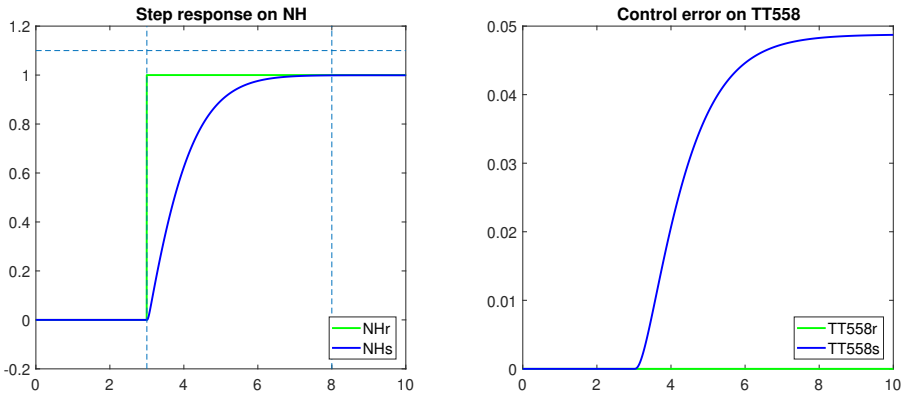

Figure 4.11: Step response on NH for PLA=90 controller, where the time constants are 10% smaller for G_{WFM}, 50% smaller for G_{A8} and 20% smaller for G_{TT558}

4.4 Global control design

4.4.1 Reference schedules

Reference values are set for the the measurement references and control signal references, as described in Section 4.2. The measurements references are for *NH* and *TT558*, while the control signal references are for *WFM*, *A8*, *FVG* and *CVG*. The sensors used for the reference schedules are described in Table 4.2, where *FRU*, NL^* and NH^* are Fuel Ratio Unit, normalized fan rotor speed and normalised compressor rotor speed, respectively.

Reference	Sensor(s)	Description
NH	*PLA,TT25*	NH^* set by *PLA*, *TT25* used to calculate NH
TT558	*PLA*	Selected operating point
WFM	*NH,TT25,PS3C*	$FRU = WFM/PS3C$ estimated from NH^*
A8	*PLA*	Selected operating point
FVG	*NL,TT1*	$NL^* = NL/\sqrt{TT1/273}$
CVG	*NH,TT25*	$NH^* = NH/\sqrt{TT25/273}$

Table 4.2: Sensors for reference schedules

Although the reference values ideally should be scheduled as a function of these sensors, introducing new sensors to the control system would introduce loops to the control system. Hence, the sensors are scheduled as a function of the *PLA* instead.

The reference values are calculated by running the existing engine model and controller, while logging the reference and sensor values for different operating points. The reference values are calculated for the operating points *PLA*=18 (GI), *PLA*=28 (FI), *PLA*=40, *PLA*=50, *PLA*=60, *PLA*=70, *PLA*=80, *PLA*=90, *PLA*=103 (IRP). The scheme of the reference schedules is presented in Figure 4.12.

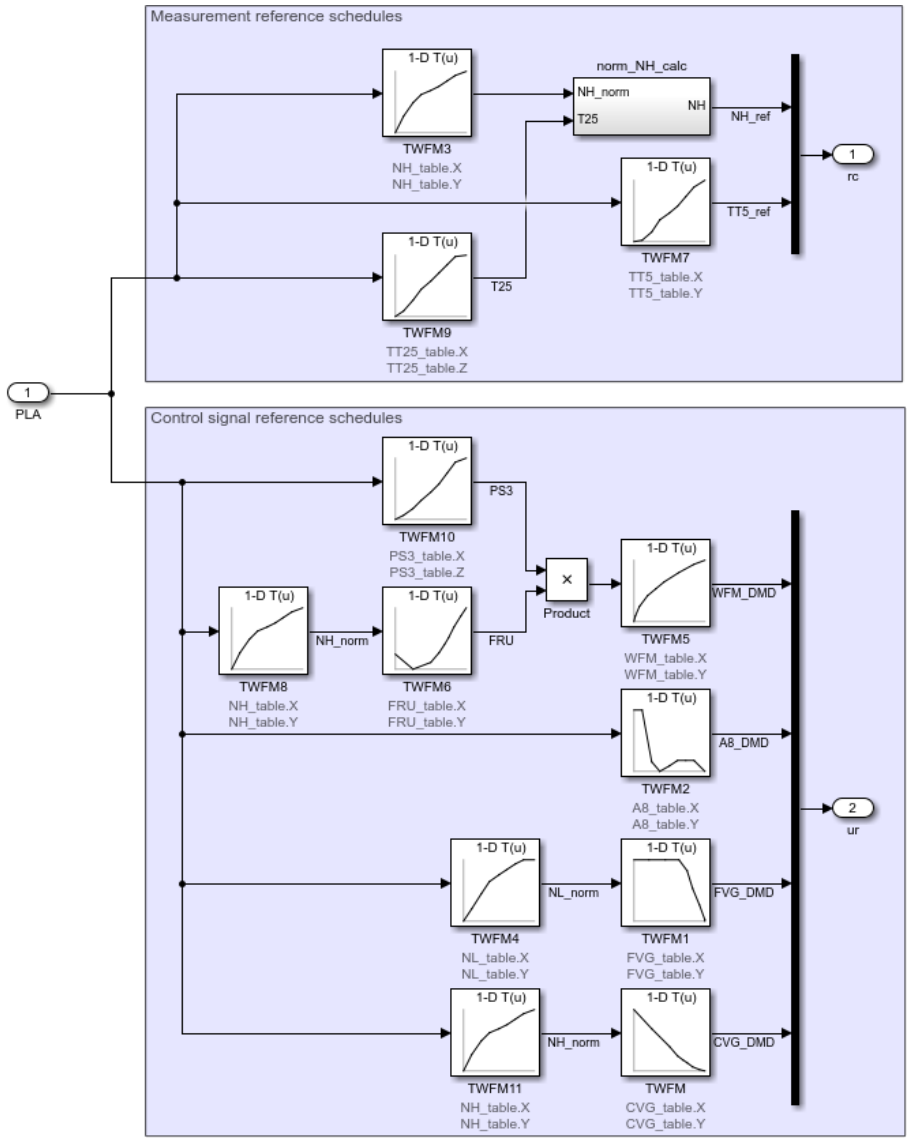

Figure 4.12: Scheme of reference value calculations

4.4.2 Gain scheduling

To cover the entire operating range, the four linear controllers designed are tied together using gain scheduling. The gain scheduling method used is to switch between the controllers as a function of some external or internal variable. The biggest disadvantage of this method is that multiple models have to be calculated in parallel, while the advantage is that it is a simple way to switch between the controllers.

The most appropriate variable to use would be the PLA, since the controllers are designed for a specific range of the PLA. However, during large transients, the value of the PLA might differ a lot from the current operating point of the engine. For example, if the PLA changes from FI to IRP the controller would switch from the PLA=28 model to the PLA=90 model directly, which would cause a bad engine response since the PLA=90 model is not designed for operating points below PLA=80.

Thus, an estimation of the current operating point of the engine, PLA^*, is scheduled as a function of NL, since the fan rotor speed is a good indication of the engine's operating point. Also, since NH is a part of the feedback control system, NL is better for this application than NH. The scheme of the gain scheduled controller is presented in Figure 4.13.

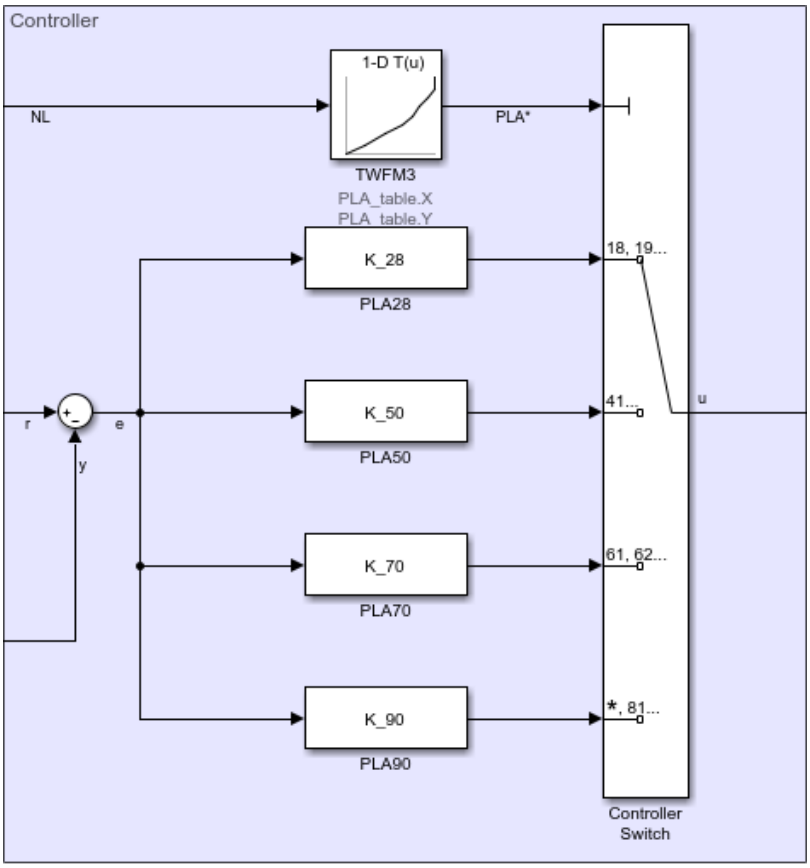

Figure 4.13: Scheme of controller scheduling

4.4.3 Bumpless transfer

A second disadvantage of the gain scheduling method used is that the different controllers produce different control signals, causing bumps to occur during controller switching. This problem is solved by implementing a bumpless transfer function.

The bumpless transfer function is implemented by feeding back the difference between the active controller and the passive controllers. The feedback is passed through a gain matrix and added to the reference errors of the controllers. Since the feedback of the active controller is zero, the active controller is unaffected by the bumpless transfer function. The bumpless transfer gain, H, is tuned in the linear case for the WFM output of the linear controllers, since the output of $A8$ does not differ a lot between the controllers. The bumpless transfer gain is selected as a diagonal matrix with as large gains as possible.

The selected bumpless transfer gain is presented in 4.9, while the scheme of the implemented bumpless transfer function is presented in Figure 4.14. Further, the resulting effect on the *WFM* control signal during a step response is seen for the four linear controllers in Figure 4.15.

$$H = \begin{bmatrix} 39 & 0 & 0 & 0 & 0 & 0 & 0 & 0 \\ 0 & 39 & 0 & 0 & 0 & 0 & 0 & 0 \\ 0 & 0 & 39 & 0 & 0 & 0 & 0 & 0 \\ 0 & 0 & 0 & 39 & 0 & 0 & 0 & 0 \\ 0 & 0 & 0 & 0 & 39 & 0 & 0 & 0 \\ 0 & 0 & 0 & 0 & 0 & 39 & 0 & 0 \\ 0 & 0 & 0 & 0 & 0 & 0 & 39 & 0 \\ 0 & 0 & 0 & 0 & 0 & 0 & 0 & 39 \end{bmatrix} \tag{4.9}$$

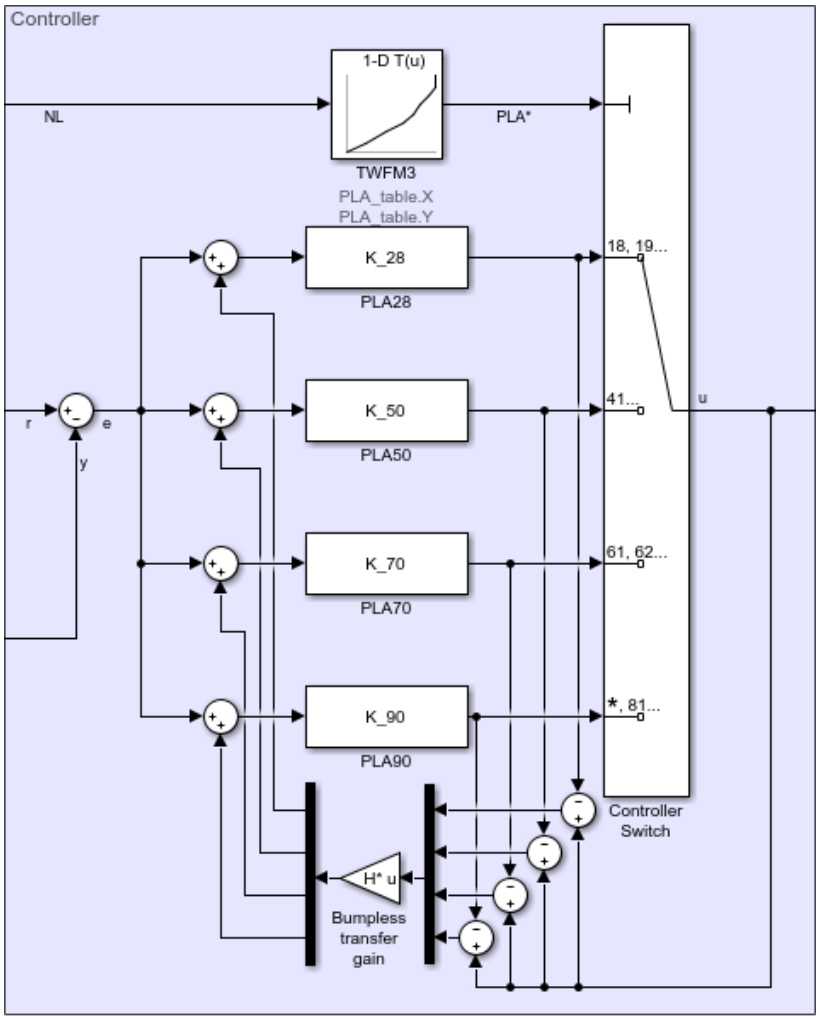

Figure 4.14: Scheme of bumpless transfer controller scheduling

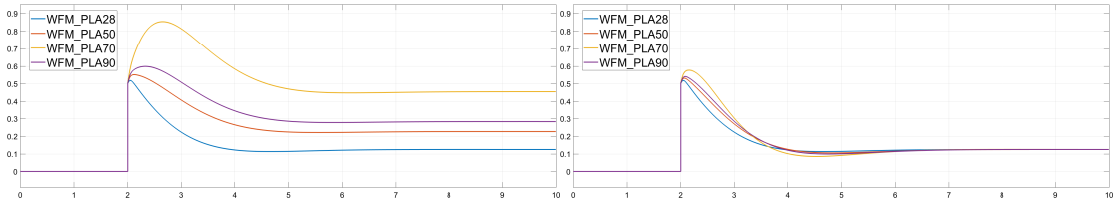

(a) PLA=28 **(b)** PLA=28 with bumpless transfer

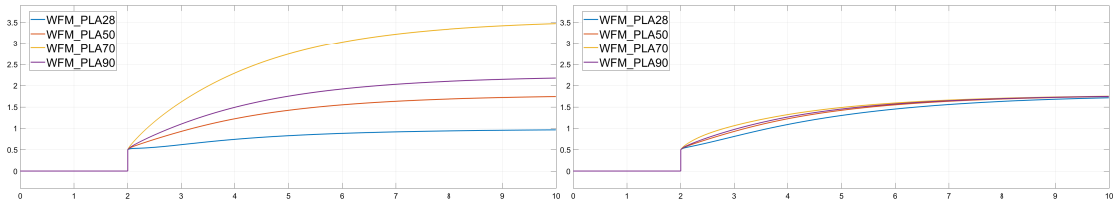

(c) PLA=50 **(d)** PLA=50 with bumpless transfer

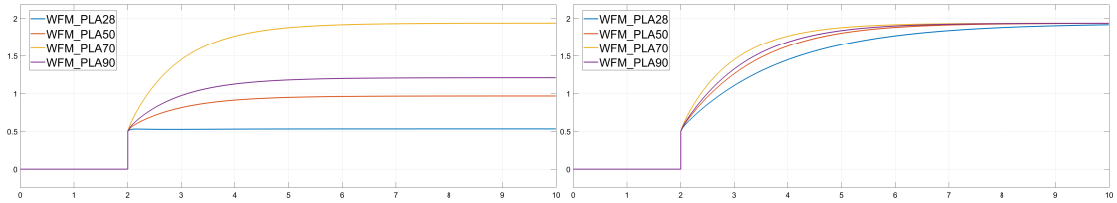

(e) PLA=70 **(f)** PLA=70 with bumpless transfer

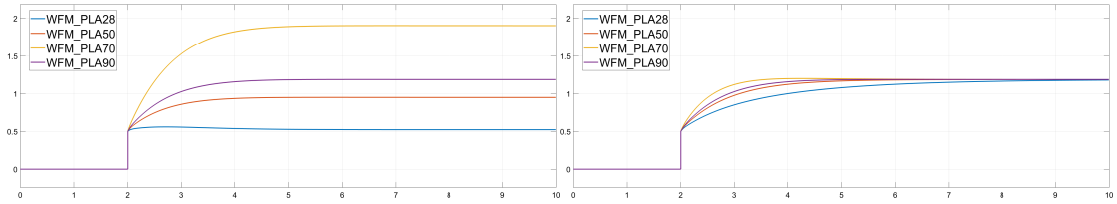

(g) PLA=90 **(h)** PLA=90 with bumpless transfer

Figure 4.15: Effect of bumpless transfer on WFM for the four linear controllers during a step response

4.4.4 Control restrictions

The fuel flow could be limited by limiting an estimate of the air to fuel ratio, which is calculated by dividing the demanded fuel flow *WFM* with the static compressor outlet pressure *PS3C*. However, to simplify the design and implementation of the control system, a rate limiter scheduled on the estimated air to fuel ratio is added to the actuator control signal of *WFM* instead. The rate limiter is tuned for the biggest transitions during normal engine operation, i.e. FI to IRP and IRP to FI.

The hardware control restrictions are simply implemented by limiting the actuator control signals to the operating range of the actuators. Although, since *FVG* and *CVG* are scheduled control signal, the hardware restriction are only implemented for the actuator control signals of *WFM* and *A8*.

However, adding the WFM rate limiter and hardware restrictions adds a saturation problem to the control system. To solve this problem the saturated signals are fed back to the bumpless transfer function, described in Section 4.4.3. The difference between the restricted actuator control signals '*ur*' and the control signal references '*ru*' are used as the active controller in the bumpless transfer function.

The scheme of the control restrictions is presented in Figure 4.16. Also, the adding of the control signal reference errors described in Section 4.2 is seen. Note that only control signal reference errors are produced for *WFM* and *A8*, leaving *FVG* and *CVG* to be scheduled as intended.

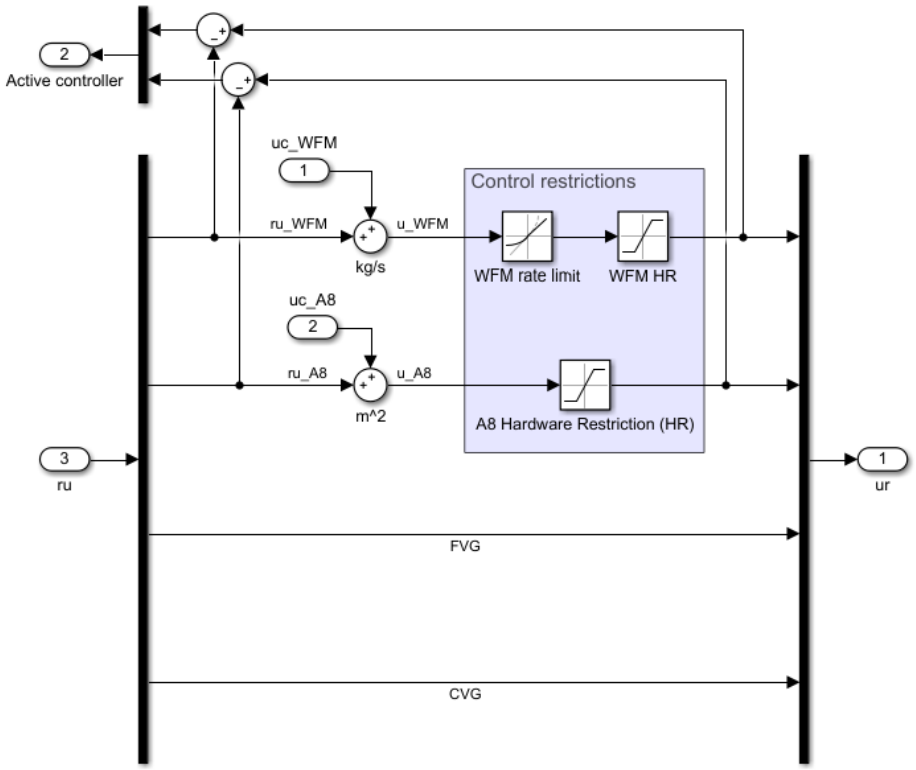

Figure 4.16: Scheme of control restrictions

5
Implementation

In this chapter the implementation of the designed control system, referred to as the MIMO SLS controller, in the existing non-linear engine model is presented. The designed control system is referred to as the MIMO SLS controller since it is a Multiple Input Multple Output (MIMO) controller designed for the low bypass aircraft engine at Sea Level Static (SLS). The MIMO SLS controller replaces the easily interchangeable FADEC software, as described in Section 1.1. The implementation of the MIMO SLS controller is presented in Section 5.1. Following this, the MIMO SLS controller is simulated and evaluated in Section 5.2. Finally, the final results are summarised and the MIMO SLS controller is discussed in Section 5.3.

5.1 Implementing the MIMO SLS controller

5.1.1 Unscaling linear controllers

The linear controllers are designed using the scaled engine model, from Section 3.2, meaning that the linear controllers are also scaled. Thus, the linear controllers of the MIMO SLS controller are unscaled to produce the correct outputs.

The inputs, or measurements y, of the linear controllers are NH and $TT558$ which have the scaling factors S_y^{NH} and S_y^{TT558}, respectively. The scaling of the inputs, to the scaled measurements y_s, is presented in (5.1). The scaled outputs, or scaled control signals u_s, of the linear controllers are WFM and $A8$ which have the scaling factors S_u^{WFM} and S_u^{A8}, respectively. The unscaling of the outputs, to the unscaled control signals u, is presented in (5.2).

$$y_s = \begin{bmatrix} S_y^{NH} & 0 \\ 0 & S_y^{TT558} \end{bmatrix}^{-1} y \tag{5.1}$$

$$u = \begin{bmatrix} S_u^{WFM} & 0 \\ 0 & S_u^{A8} \end{bmatrix} u_s \tag{5.2}$$

The scheme of the implemented unscaling of the linear controllers is shown in Figure 5.1. Note that the active controller of the bumpless transfer function is acquired from after the control restrictions, as described in section 4.4.4, and scaled to the units of the scaled controller.

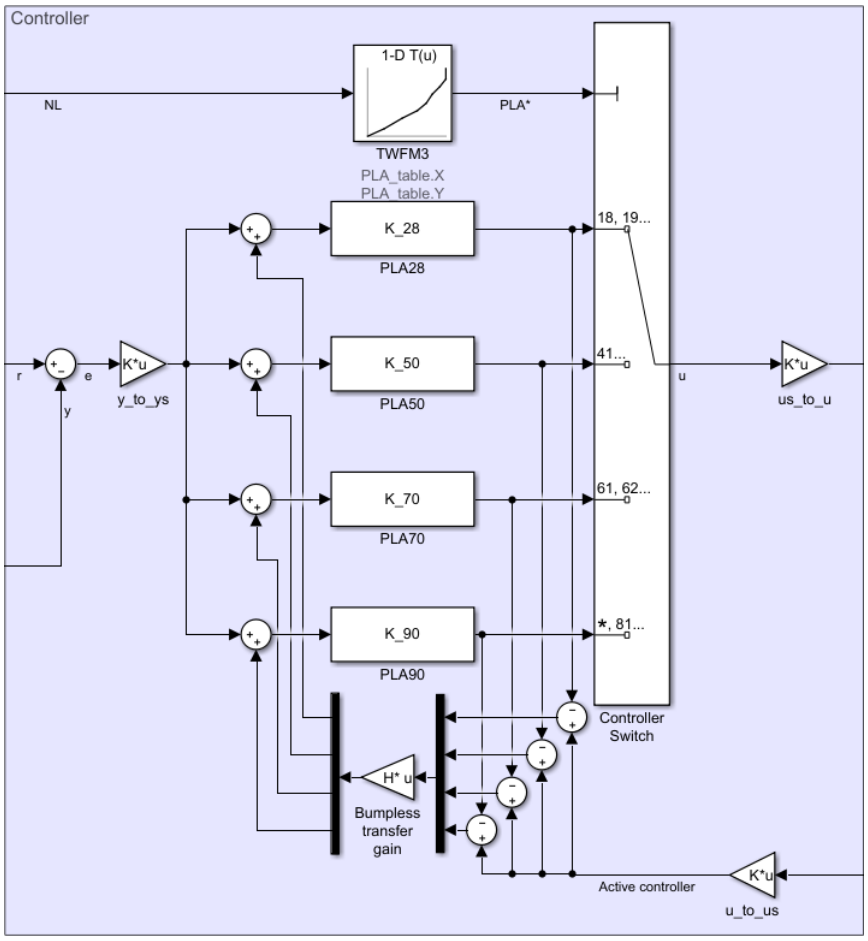

Figure 5.1: Scheme of unscaled linear controllers

5.1.2 I/O signal conversion

The inputs of the MIMO SLS controller are *PLA*, *NL*, *NH*, *TT558* and *PS3C*. The equivalent inputs of the FADEC software are of different units than the MIMO SLS controller. Thus, the inputs of the FADEC software are extracted and converted to the matching units. The input unit conversion is presented in Table 5.1.

Input	FADEC Unit	MIMO SLS unit
PLA	% stroke	degree
NL	Hz	Hz
NH	Hz	Hz
TT558	ohm	K
PS3C	psi	kPa

Table 5.1: Input unit conversion of MIMO SLS controller

However, the outputs *WFM*, *A8*, *FVG* and *CVG* of the MIMO SLS controller are more complicated. The control signal references '*ru*' of the MIMO SLS controller have matching units to the FADEC software (% stroke), but the control signal reference errors '*uc*' do not. Thus, to add the control signal reference errors to the

control signal references, the conversion presented in Figure 5.2 is performed. The control signal references are converted to the units of the control signal reference errors, where the two signals are added together. Following this, the resulting outputs are converted back to the correct units (% stroke).

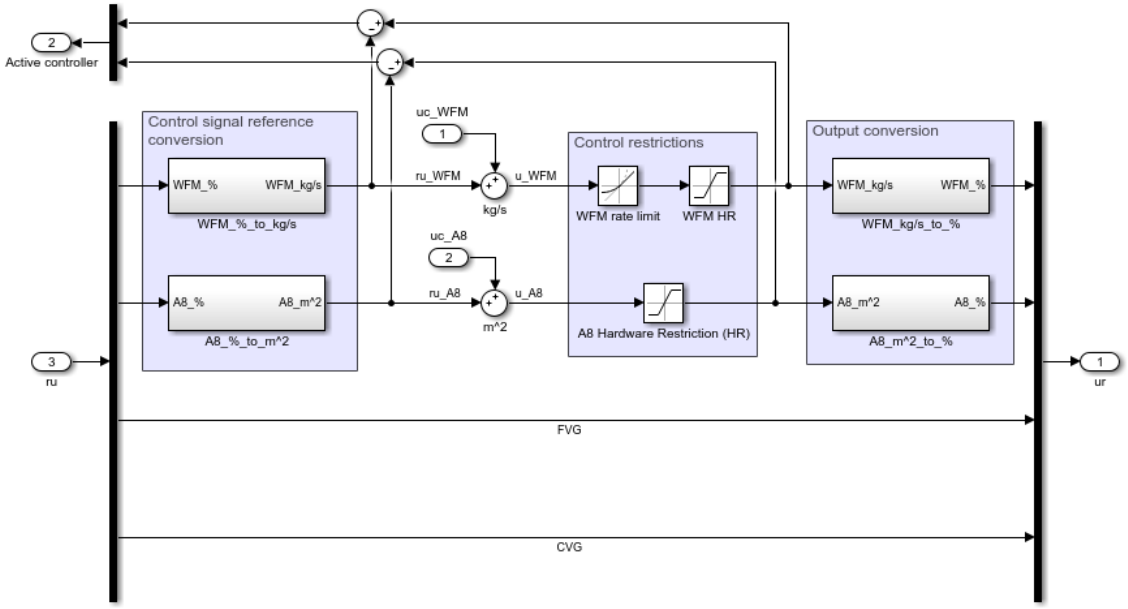

Figure 5.2: Scheme of output unit conversion for MIMO SLS controller

5.2 Control system evaluation

The implemented MIMO SLS controller is evaluated by performing various simulations with the existing non-linear engine model. The simulations are also performed with the FADEC software for comparison. The simulations are divided into two categories, linear simulations and non-linear simulations. The linear simulations are performed within the operating ranges of the linear controllers, to evaluate the performance of the linear controllers. The non-linear simulations are performed throughout the entire operating range, to evaluate the performance of the gain scheduling and bumpless transfer. However, since all simulations are started from the operating point GI (PLA=18), the first parts of some simulations are omitted.

The interesting engine I/Os to plot are the inputs *NL*, *NH* and *TT558* as well as the outputs *WFM* and *A8*, since these I/Os are used by the MIMO SLS controller to control the engine. Also, the I/Os are scaled by the respective operating ranges, meaning that the operating ranges for all I/Os are between 0 and 1 in the following plots.

5.2.1 Linear simulations

Reference tracking and transient performance

To evaluate the reference tracking and transient performance of the linear controllers, the following simulations are performed. Three different operating points within the linear controllers operating range, with step changes between the operating points, are set for each simulation. The transients of the linear controllers are evaluated for the step changes between the different operating points. The operating points used for the different linear controllers is presented in Table 5.2. The interesting engine I/Os for the reference tracking and transient performance simulations are presented in Figure 5.3.

Linear controller	**OP 1**	**OP 2**	**OP 3**
PLA=28	PLA=18	PLA=28	PLA=35
PLA=50	PLA=45	PLA=50	PLA=55
PLA=70	PLA=65	PLA=70	PLA=75
PLA=90	PLA=85	PLA=90	PLA=103

Table 5.2: Simulated operating points (OP) of the linear controllers

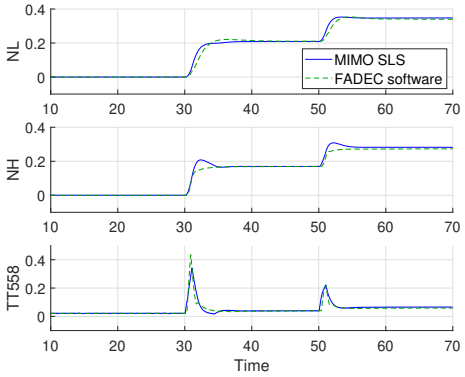

(a) Measurements - PLA=28

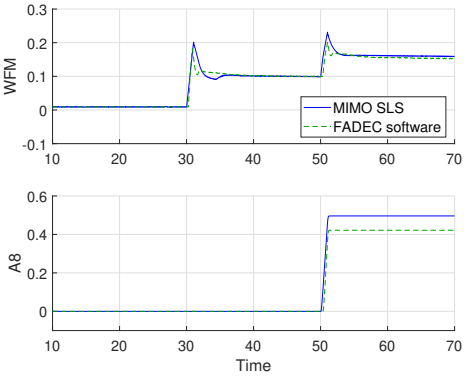

(b) Control signals - PLA=28

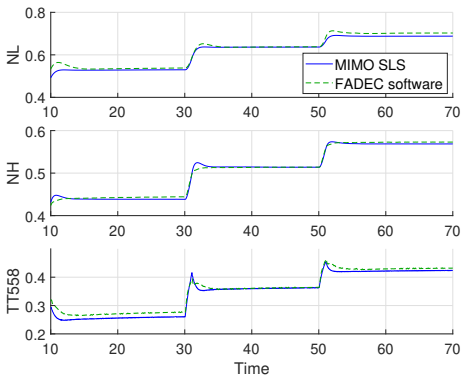

(c) Measurements - PLA=50

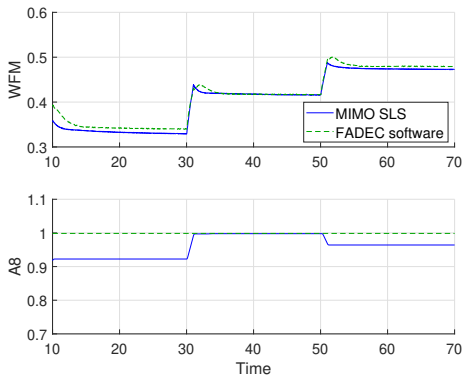

(d) Control signals - PLA=50

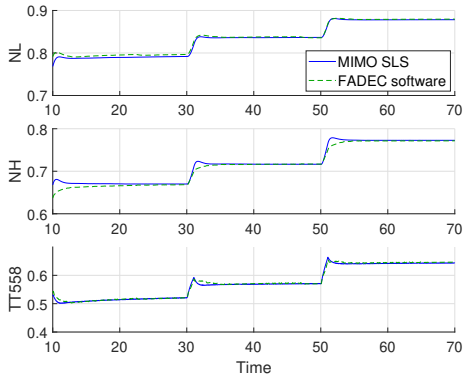

(e) Measurements - PLA=70

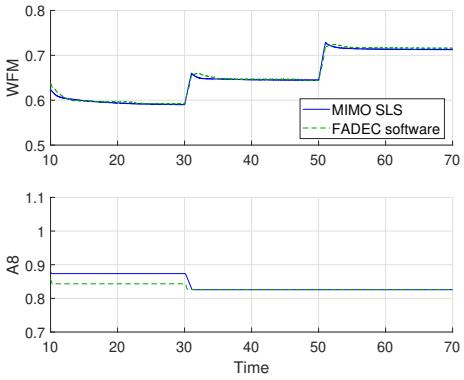

(f) Control signals - PLA=70

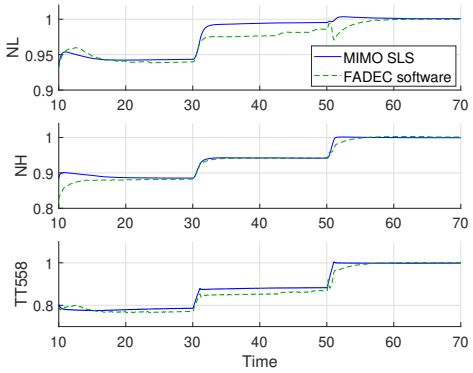

(g) Measurements - PLA=90

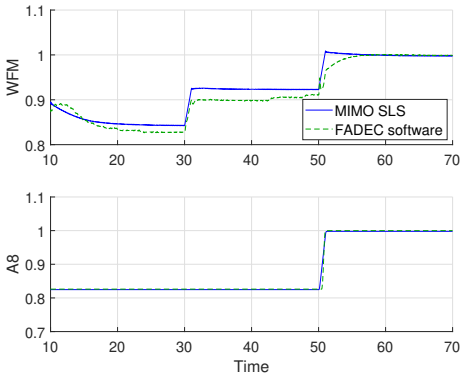

(h) Control signals - PLA=90

Figure 5.3: Reference tracking performance of the linear controllers

The simulations indicate that good reference tracking is achieved for all linear controllers. Also, even though the fan rotor speed NL is not included in the feedback control loop, the behavior of NL in the MIMO SLS controller is similar to the FADEC software. The transients of the step responses, between the operating points, are fast and without excessive overshoots. The biggest overshoots seen is the step responses of the linear controller for PLA=28, which are still reasonably small.

Disturbance attenuation

To evaluate the disturbance attenuation of the linear controllers, a disturbance is simulated in the operating points used as design points for every linear controller. The chosen disturbance for the simulations is air bleed extraction, since it is a large disturbance. Yuhas and Ray [20] present the effects of air bleed extraction on thrust levels for the low bypass aircraft engine F404-GE-400. Since the engine model used in this thesis is very similar to the F404-GE-400 engine, the same air bleed extraction effects are used in the simulations. The air bleed extraction effects for the simulated operating points are presented in Table 5.3.

PLA	**Air bleed effect**
28	6%
50	7%
70	7%
90	3.5%

Table 5.3: Effects of air bleed extraction at the simulated operating points

The simulations are performed by setting and maintaining the operating point of the simulated controller until stabilised, followed by adding the air bleed extraction effect for the operating point as a step response. The interesting engine I/Os for the disturbance attenuation simulations are presented in Figure 5.4. The plots start at time t seconds, where the operating point is stabilised, and the step response of the disturbance occur at time $t + 2$ seconds.

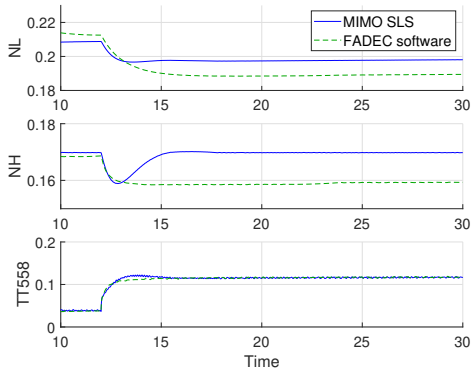

(a) Measurements - PLA=28

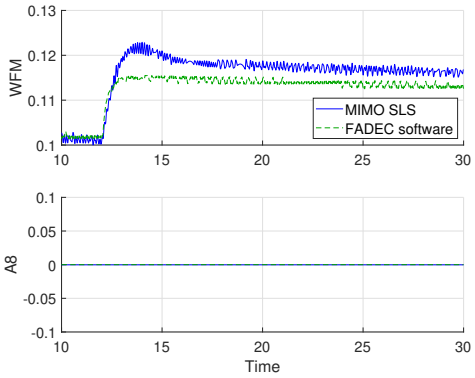

(b) Control signals - PLA=28

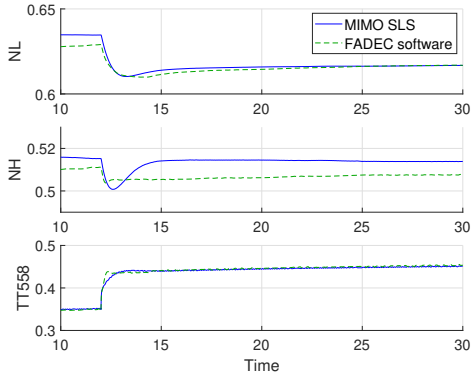

(c) Measurements - PLA=50

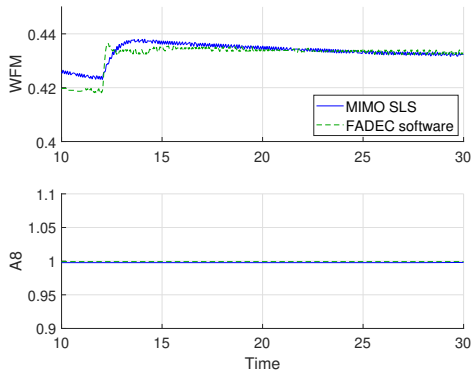

(d) Control signals - PLA=50

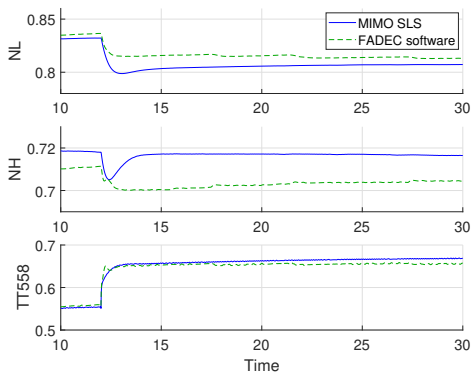

(e) Measurements - PLA=70

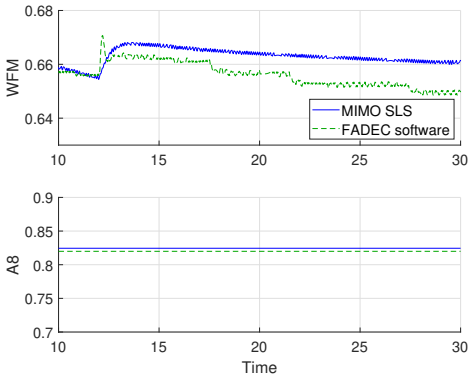

(f) Control signals - PLA=70

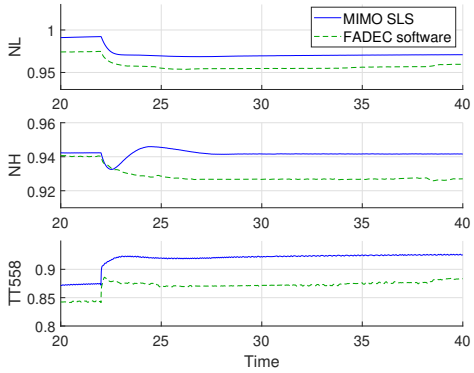

(g) Measurements - PLA=90

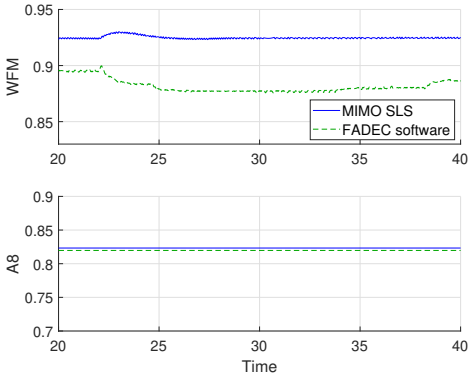

(h) Control signals - PLA=90

Figure 5.4: Disturbance attenuation of the linear controllers

The simulations indicate that good disturbance attenuation is achieved, since the reference value of NH is quickly recovered. Also, the simulations reveal that the MIMO SLS controller handles disturbances better than the FADEC software does. However, this is expected since the FADEC software does not have any integral action.

5.2.2 Non-linear simulations

Transients between linear controllers

To evaluate the performance of the controller scheduling and bumpless transfer, the following simulation is performed. The simulation performs step responses to the four operating points used as design points of the linear controllers, which are PLA=28, PLA=50, PLA=70 and PLA=90. In the transients between these step responses, the control scheduling takes place and the response of the transients can be evaluated. Also, the smoothness of these transients determine how well the bumpless transfer performs. The interesting engine I/Os for the simulation of the transients between linear controllers are presented in Figure 5.5.

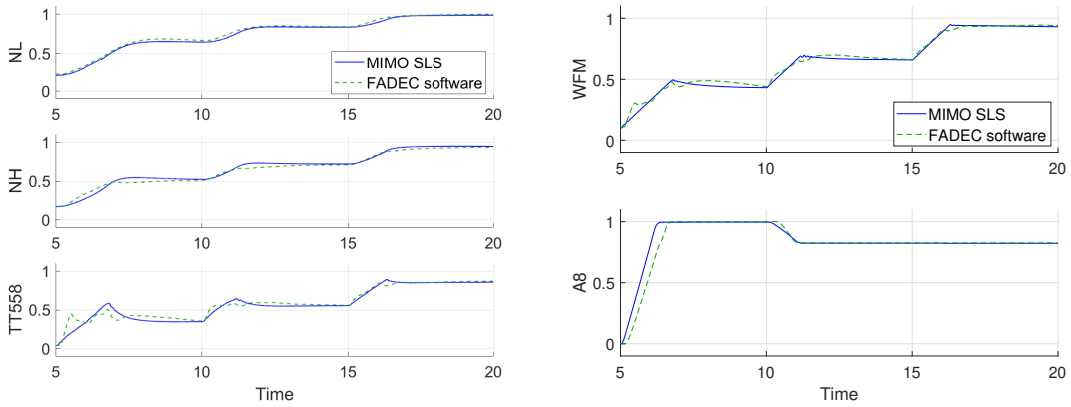

(a) Measurements **(b)** Control signals

Figure 5.5: Transient performance of the MIMO SLS controller

The simulation indicate that good controller scheduling and bumpless transfer is achieved, since the transients between the linear controllers are fast and smooth. The biggest difference seen is that the MIMO SLS controller slightly overshoots the reference values of the compressor rotor speed *NH*, while the FADEC software slightly undershoots the reference values. However, this difference is still considered to be reasonably small.

Engine thrust response

To evaluate the control systems thrust response to the engine, as well as the control systems performance to a large and fast transient. This simulation performs a step response from the operating point FI (PLA=28) to the operating point IRP (PLA=103), also defined as the thrust response of the engine. The interesting engine I/Os for the engine thrust response simulation are presented in Figure 5.6

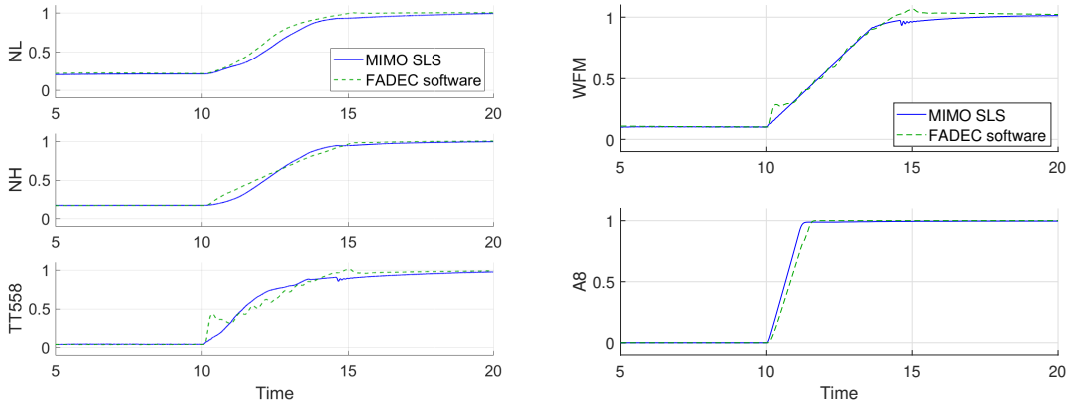

(a) Measurements **(b)** Control signals

Figure 5.6: Engine thrust response performance of the MIMO SLS controller

The thrust response of the engine is close to 5 seconds, thus fulfilling the control requirements described in Section 4.1. The large and fast transient is smooth, indicating that good controller scheduling and bumpless transfer is achieved for fast transients as well. Additionally, the WFM rate limiter's upper limit, described in Section 4.1, is tuned to this case. This can be seen since the control signal *WFM* for the global controller increases with similar rate as for the FADEC software.

Engine pulse response

To evaluate the decreasing rate of the control signal *WFM* a pulse response is simulated, i.e from the operating point FI (PLA=28) to the operating point IRP (PLA=103) and then back to FI. The interesting engine I/Os for the engine pulse response simulation are presented in Figure 5.7.

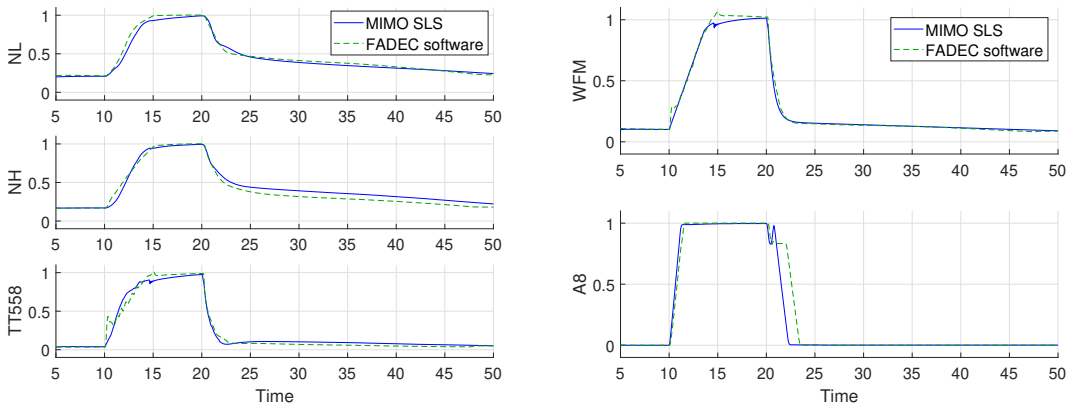

(a) Measurements **(b)** Control signals

Figure 5.7: Engine pulse response performance of the MIMO SLS controller

The simulation indicate that the engine pulse response behaves as expected, since the global controller follows the FADEC software for all inputs and outputs relatively close. Further, since the control signal *WFM* for the global controller decreases with similar rate as the FADEC software, it can be seen that the *WFM* rate limiter's lower limit, described in Section 4.1, is tuned to this case.

Engine variations

To evaluate the robustness of the control system, engine variations are simulated by varying the component efficiencies of the engine. Three different engines are simulated, one with nominal component efficiencies, one with good component efficiencies and one with bad component efficiencies. All engines are simulated for the thrust response simulation and compared to evaluate the robustness of the MIMO SLS controller. The interesting engine I/Os for the simulation with engine variations are presented in Figure 5.8.

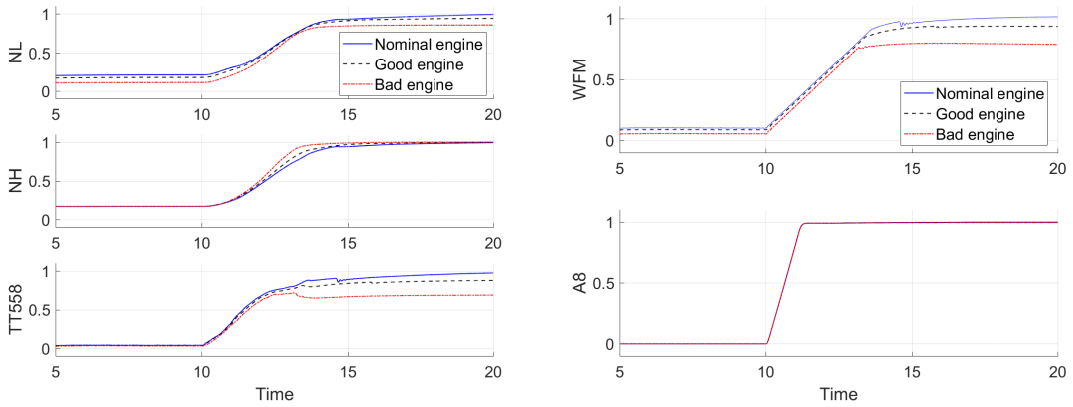

(a) Measurements **(b)** Control signals

Figure 5.8: Robustness performance of the MIMO SLS controller

The simulation indicate that a robust control system is achieved, since the reference for *NH* is maintained for all three engines. However, the fan rotor speed *NL* decreases as the component efficiencies of the engine decreases. Although, this is to be expected since *NL* is not included in the feedback loop of the control system.

5.3 Summary and discussion

This section summarises the final result and the control system design for the low bypass aircraft engine. Different control strategies and control designs were reviewed in the literature survey, in Chapter 2, to selected the methods used in the control system design of this thesis. The I/O selection selection method RHP-zeros was a simple and effective way to rule out many I/O pairs. Further, the RGA method was an effective way to select the control configuration of the control system. However, since these methods do not take application specific aspects into consideration, these methods were combined with application specific knowledge in Chapter 3.

When designing the linear controllers, in Chapter 4, the popular H_∞ methodology was used. The H_∞ controllers were designed using MATLAB's tool H-Infinity Synthesis, available in the Robust Control Toolbox [19]. The H-Infinity Synthesis tool worked well for this application and was simple to use. Provided examples of how to use the H-Infinity Synthesis tool were very helpful during the development of the augmented plant in MATLAB. The biggest benefit of using the H-Infinity Synthesis tool was the simple tuning possibilities, since the augmented plant with the weighting functions was implemented in MATLAB. Also, plots could be added to the script, which led to fast and simple evaluation of the selected weighting functions.

One disadvantage of the H_∞ methodology is that it results in high order controllers. Even though the linear engine model was reduced heavily, the linear controllers designed in this thesis are of order 13, which is relatively low for an H_∞ controller. That being said, the scaling and reduction of the linear engine model proved to

reduce the order of the resulting controller without effecting the performance of the controller much. Further, the MATLAB tools used for the scaling and reduction proved to be sufficient.

The linear controllers performed well for both the linear and non-linear engine models, maintaining a given reference value with fast response time for the *NH* control loop. Good disturbance attenuation of the linear controllers was also achieved, since the reference values for *NH* were held during large disturbances. Also, the controller minimized the control error of *TT558*, thus fulfilling the control requirements from Section 4.1. The worst performing controller was the linear controller for operating point PLA=28. However, even though this controller had some overshoots during transients, they were still within the control requirements.

The global control system presented in Chapter 4 also performed well, with fast and smooth transients between the linear controllers. The gain scheduling worked well, by switching controllers depending on the fan rotor speed *NL*, which was a good indication of the engine's current operating point. The smooth transients between the gain scheduled controllers indicated that the implementation of the bumpless transfer function improved the smoothness of the transients. Also, a robust control system that could handle engine variations was achieved, fulfilling the control requirements from Section 4.1.

However, as described in Section 2.1, the control system of a low bypass aircraft engine is a complex control problem. To reduce the complexity of the control system, some simplifications were made. One being that the engine used in this thesis is operating in SLS, as described in Section 1.1, meaning that the full flight envelope is not considered. Although, when designing a control system for the full flight envelope, a similar gain scheduling approach could be used with additional linear controllers for the new operating points.

Finally, in Chapter 5, the implementation of the MIMO SLS controller in the FADEC model proved that the control system could be implemented on the real engine. This could be done by generating the code of the MIMO SLS controller in MATLAB/Simulink to replace the code of the FADEC software. Although, before the MIMO SLS controller is implemented on the real engine, the simplifications made in this thesis should be considered to ensure safe engine operation.

Bibliography

[1] J. Städje, "Reaktionsmotor 12 - både vacker och stark," 2008. Available at:https://techworld.idg.se/2.2524/1.174315/reaktionsmotor-12---bade-vacker-och-stark

[2] M. Harefors, "A Study in Jet Engine Control," 1999 Avaliable at: ISBN 91-7197-828-3

[3] M. Harefors, "Control structure design methods applied to a jet engine," Proceedings of the 1999 IEEE International Conference on Control Applications (Cat. No.99CH36328), Kohala Coast, HI, USA, 1999, pp. 45-50 vol. 1, doi: 10.1109/CCA.1999.806141.

[4] R. Samar and I. Postlethwaite, "Multivariable controller design for a high performance aero-engine," 1994 International Conference on Control - Control '94., Coventry, UK, 1994, pp. 1312-1317 vol.2, doi: 10.1049/cp:19940326.

[5] Y. Luo, H. Liu, L. Jia and W. Cai, "A practical guideline to control structure selection for MIMO processes," 2011 IEEE International Conference on Automation and Logistics (ICAL), Chongqing, China, 2011, pp. 405-410, doi: 10.1109/ICAL.2011.6024752.

[6] A. E. Sutton, "Application of multivariable control to a turbofan engine," International Conference on Control 1991. Control '91, Edinburgh, UK, 1991, pp. 1041-1048 vol.2.

[7] J.Szuch, James Soeder, K. Seldner, D. Cwynar, "F100 multivariable control synthesis program: Evaluation of a multivariable control using a real-time engine simulation," 1977.

[8] S. A. Eisa and H. P. Tyler, "Closed Loop Control of an Afterburning F100 Gas Turbine Engine," 1986 American Control Conference, Seattle, WA, USA, 1986, pp. 266-272, doi: 10.23919/ACC.1986.4788946.

[9] W. H. Pfeil, M. Athans and H. A. Spang, "Multi-Variable Control of the GE T700 Engine using the LQG/LTR Design Methodology," 1986 American Control Conference, Seattle, WA, USA, 1986, pp. 1297-1312, doi: 10.23919/ACC.1986.4789132.

[10] S. S. Mahil and S. Bommaraja, "A low order optimal controller for a turbofan jet engine," Conference Record of the 1992 IEEE Industry Applications Society Annual Meeting, Houston, TX, USA, 1992, pp. 1717-1720 vol.2, doi: 10.1109/IAS.1992.244229.

[11] P. J. Deore and B. M. Patre, "Design of robust compensator for jet engine: an interval analysis approach," Proceedings of 2005 IEEE Conference on Control Applications, 2005. CCA 2005., Toronto, ON, Canada, 2005, pp. 376-381, doi: 10.1109/CCA.2005.1507154.

[12] A. -N. Tudosie, "Embedded control system for an aircraft two-spool jet engine with coolant injection into the compressor," 2018 19th International Carpathian Control Conference (ICCC), Szilvasvarad, Hungary, 2018, pp. 389-394, doi: 10.1109/CarpathianCC.2018.8399661.

[13] G. L'Erario et al., "Modeling, Identification and Control of Model Jet Engines for Jet Powered Robotics," in IEEE Robotics and Automation Letters, vol. 5, no. 2, pp. 2070-2077, April 2020, doi: 10.1109/LRA.2020.2970572.

[14] A. Nobakhti and N. Munro, "Design of a novel simply structured mixed-sensitivity loop-shaping robust controller for a gas-turbine," Proceedings of the 2004 American Control Conference, Boston, MA, USA, 2004, pp. 4625-4630 vol.5, doi: 10.23919/ACC.2004.1384040.

[15] M. Hardt, J. W. Helton and K. Kreutz-Delgado, "Numerical solution of nonlinear H_2 and H_∞ control problems with application to jet engine compressors," in IEEE Transactions on Control Systems Technology, vol. 8, no. 1, pp. 98-111, Jan. 2000, doi: 10.1109/87.817695.

[16] H. Wang, L. Ouyang, D. Wang and L. Liu, "Multivariable robust control design of a turbofan engine for full flight envelope operation," The 2010 IEEE International Conference on Information and Automation, Harbin, China, 2010, pp. 2121-2125, doi: 10.1109/ICINFA.2010.5512199.

[17] C.W. Jones, P.J. Fleming, Controller Design for a Gas Turbine Engine, IFAC Proceedings Volumes, Volume 12, Issue 7, 1979, Pages 619-623, ISSN 1474-6670, https://doi.org/10.1016/S1474-6670(17)65660-X. (`https://www.sciencedirect.com/science/article/pii/S147466701765660X`)

[18] The MathWorks, Inc. (2017). MATLAB Version: 9.2.0.538062 (R2017a). Accessed: February 20, 2023. Available: `https://www.mathworks.com/`.

[19] The MathWorks, Inc. (2017). Robust Control Toolbox: 6.3 (R2017a). Accessed: February 20, 2023. Available: `https://se.mathworks.com/help/robust/controller-synthesis.html?s_tid=CRUX_lftnav`

[20] Andrew J. Yuhas and Ronald J. Ray, "Effects of Bleed Air Extraction on Thrust Levels of the F404-GE-400 Turbofan Engine", presented at the AIAA Joint Propulsion Conference, Nashville, TN, USA, July 1, 1992, Document ID 19920020182.

DEPARTMENT OF ELECTRICAL ENGINEERING
CHALMERS UNIVERSITY OF TECHNOLOGY
Gothenburg, Sweden
www.chalmers.se

CHALMERS
UNIVERSITY OF TECHNOLOGY